Article

Fine-Grained Lithofacies Types and Sedimentary Model of the Upper Permian Longtan Formation Coal Measures in the Western Guizhou Region, South China

Xiaoming Li, Xuan Tang,* Shaobin Guo, Jinchuan Zhang, Ende Deng, and Chaoli Lan

Read Online

ACCESS | Metrics & More | Article Recommendations

ABSTRACT: The upper Permian Longtan Formation is widely distributed in southwestern China and is well known for multilayer coal and high organic shale, with significant shale gas potential that has yet to be fully explored and developed. The Longtan coal-bearing strata are composed of complex lithological assemblages of fine-grained sedimentary rocks such as sandstone, coal, shale, and limestone, which exhibit significant differences from marine shale. To better understand the organic-rich lithofacies, their distribution, and their controlling factors, this study carried out a detailed survey of the outcrop and drill cores in the western Guizhou region and examined the fine-grained lithofacies, their assemblages, and their geochemical characteristics. The results showed that (1) the total organic carbon of the Longtan Formation shale in western Guizhou ranged from 1.44 to 14.79%, with an average of 6.41%, and the organic matter was mainly composed of vitrinite. The mineral composition was mainly clay minerals and brittle minerals; the clay minerals were mainly composed of kaolinite (average 11.13%) and illite/smectite mixed layers (average 26.69%) and the brittle minerals were mainly composed of quartz (average 31.63%) and feldspar (average 12.88%). (2) Eight types of lithofacies were identified, including silty mudstone, muddy siltstone, carbonaceous mudstone, carbonaceous shale, bioclastic-bearing mudstone, bioclastic-bearing sandstone, fine sandstone, and coal seam. (3) The six typical lithofacies assemblages were developed in the Longtan Formation, which represented different sedimentary environments of the marine−continental transitional facies in the study area. The lithofacies assemblages A and C represent sedimentation in the lagoon environment. The lithofacies assemblage B represents peat swamp facies. The lithofacies assemblage D represents a tidal flat facies peat flat-mixed flat-sand flat sedimentary environment. The lithofacies assemblage E and F represent the delta sedimentary environment. (4) The sedimentary model of the Longtan Formation in western Guizhou was predominantly deltaic and tidal flat sedimentary systems. Lithological and lithofacies studies of Longtan fine-grained rocks were used to provide a geological framework for examining the fine grain deposition distribution and shale gas resource evaluation. This study is highly important for understanding the sedimentology and oil and gas exploration in the region, providing a basis for identifying and exploring coal-bearing shale gas potential and a reference for the analysis of shale in the world's continental transitional areas.
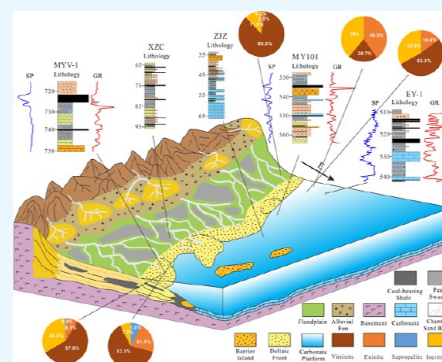
1. INTRODUCTION

In recent years, China's shale gas industry has entered a period of rapid development, with significant breakthroughs in shale gas exploration and development, causing China to be the third country to achieve shale gas industrial production after the United States and Canada.[1−3] According to the latest resource assessment results, China has a large amount of shale gas resources, with recoverable resources of 12.85 trillion cubic meters.[4−7] With the successful commercial development of marine shale gas in southern Sichuan, shale gas will become an important part of China's future energy types.[4,8,9] Previous researchers have studied the geochemical and reservoir characteristics of the Longtan Formation shale in western Guizhou and evaluated its shale gas potential, showing enormous potential and exploration prospects.[10−18] However,

the exploration, development, and research of marine−continental transitional shale gas in China is still in its early stages, there are still many problems, and no significant breakthroughs have been made.[19−21]

The Longtan Formation in western Guizhou is a marine−continental transitional sedimentary environment of lagoon-tidal flat and deltaic sedimentary facies.[22−26] The area has high organic matter content, mainly type III kerogen, and has a
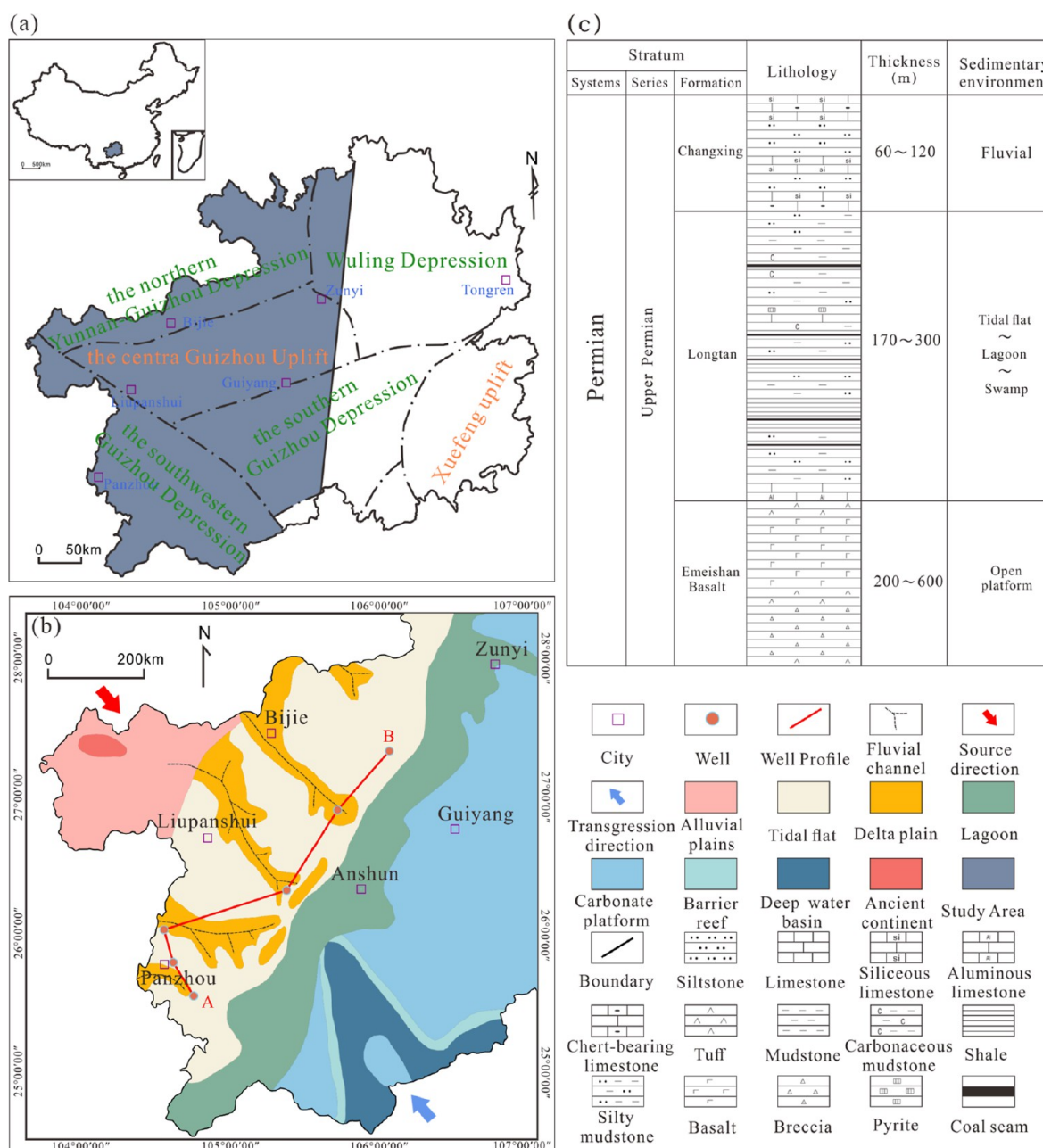
Figure 1. (a) Tectonic location of the study area and division of regional tectonic units. Adapted with permission from ref 44. Copyright 2021 Energy Sci. Eng. Rev.; (b) paleogeographic map of late Permian sediment in the study area. Adapted with permission from ref 11. Copyright 2019 Miner. Rev.; (c) stratigraphy in the study area of the late Permian region. Adapted with permission from ref 44. Copyright 2021 Energy Sci. Eng. Rev.

good material basis for shale gas enrichment,[14,18,27,28] with high gas production potential.[27,29] Six types of mudstone facies have been identified in the Longtan Formation in western Guizhou, including carbonaceous mudstone, siliceous-clay mixed mudstone, argillaceous mudstone, silty shale, muddy siltstone, and calcareous-clay mixed shale.[30] Previous scholars classified the Longtan Formation shale in the Sichuan Basin and its surrounding areas based on its mineral content and organic matter abundance.[18,31,32] The facies classification of marine shale is relatively mature,[33−38] but in the marine−continental transitional environment, shale rich in organic matter has not been sufficiently studied for facies classification and targeted research. Moreover, there is a lack of research on the changes in vertical lithofacies, organic matter content,

organic matter type, and mineral content variations in the different sedimentary environments in the Longtan Formation in our study area.

To address existing issues, detailed field outcrop observations, thin section identification, X-ray diffraction analysis, total organic carbon analysis, and other techniques are conducted to systematically sample and analyze shale in typical sedimentary environments, such as the delta and tidal flats in the western Guizhou area. The different types and characteristics of shale facies in different sedimentary environments are compared to gain a deeper understanding of the differences in organic matter and reservoir properties of shale in the Longtan Formation containing coal seams. This research aims to provide a basis for identifying and exploring shale gas potential

in this area and a reference for the analysis of marine—continental transitional sedimentary environment shale in the world.

2. GEOLOGICAL BACKGROUND

Guizhou Province is divided into six primary geological units, from south to north (Figure 1a).[29,39] The study region is located in the Western Guizhou Depression and the Guizhong Uplift, which are on the southern edge of the Yangtze platform and adjacent to the South China Fold Belt.[40] This region has undergone six major tectonic cycles: the Yangtzeian Cycle, Caledonian Cycle, Hercynian Cycle, Indosinian Cycle, Yanshanian Cycle, and Himalayan Cycle, which can be further divided into six stages: basement formation stage (Pt_2–Pt_3), passive continental margin stage (Z–S), intracontinental rift stage (D–P), stable platform stage (T_1–T_2), intracontinental mountain-building stage (T_3–K_1), and compressional uplift stage (K_2–Q).[41−43]

The Longtan Formation coal measures are mainly preserved in large synclines or synclinores such as the Panguan syncline. Based on the differences in structural deformation, the western Guizhou area is divided into the Zijin-Nayong NE-trending structural deformation zone, the Shuicheng-Ziyun NW-trending structural deformation zone, and the complex structural deformation zone in southwestern western Guizhou.[45] The Zijin-Nayong NE-trending structural deformation zone is mainly characterized by NE-trending folds and faults. The Shuicheng-Ziyun NW-trending structural deformation zone is a strip-shaped distribution with a length of approximately 250 km and a width of approximately 40 km and is mainly characterized by NW-trending folds and thrust faults. The complex structural deformation zone in southwestern western Guizhou is characterized by NW-trending folds and faults, NE-trending folds and faults, near-NS and near-EW trending structures, and multiple groups of composite superimposed structures, forming various structural forms such as the Langdai triangle, the Fa'er rhombus, the Panxian triangle, and the Qinglong arc.[46] The fold structures in the area are gently and widely distributed, exhibiting a short-axis pattern.[45]

The sedimentary environment in western Guizhou has undergone significant changes, with multiple small-scale transgressions and regressions occurring from the Carboniferous to the Permian.[47] In the late Carboniferous, the ancient Kangding-Yunnan land slowly uplifted, and seawater invaded the eastern and southeastern parts of the study area, with extensive coastal lagoon development. The western Guizhou area was predominantly dominated by carbonate platforms. In the early Permian, large amounts of debris from the ancient Kangding-Yunnan land entered the basin after weathering, and the seawater retreated in the northeast direction. The sedimentary environment changed to tidal flats, swamps, and delta systems, predominantly dominated by delta-tidal-flat systems. In the late Permian, the sedimentation rate in the coal basin slowed down, the supply of sediment decreased, and the rising sea level caused transgressions that caused the coal-accumulating environment to shift westward.[28,48] The western Guizhou area was predominantly dominated by delta and tidal flat systems (Figure 1b).

3. SAMPLING AND EXPERIMENTAL METHODS

Outcrop observations were carried out in the study area, which included three outcrop sections and two drilling wells in the northwest to southeast direction of the study area, as shown in Figure 1. A total of 89 samples were collected, all of which were core samples from the Longtan Formation of the MY101 well in the study area. Experimental methods such as thin section observation, coal petrographic analysis, X-ray diffraction analysis, and determination of total organic carbon content were carried out.

3.1. Thin Section Observation. Thirty-five polished thin sections were prepared using standard techniques for petrographic analysis following the China National Petroleum and Natural Gas Industry Standard GB/T 35206-2017.[49] The thin sections of rocks were observed under transmitted light using a Zeiss Axioskop 40 optical microscope.

3.2. Organic Petrography. Thirty-five shale thin sections were prepared using standard techniques for organic maceral identification and analysis. The thin sections of rock coal were observed under reflected light using a DM4500P microscope produced by Leica under oil immersion lens conditions. Observation conditions and criteria followed the China National Petroleum and Natural Gas Industry Standard SY/T 6414-2014.[50]

3.3. X-ray Diffraction Analysis. X-ray diffraction (XRD) is a commonly used method for determining the mineral composition of rocks. First, the rock sample is ground into a powder form in an agate mortar with an average particle size of approximately 5 μm or less than 200 mesh. Second, the powdered sample is pressed into a mold and then tested to obtain the mineral mass percentage.[51] The experiment was carried out in the XRD powder crystal laboratory of the Scientific Research Institute of China University of Geosciences (Beijing) using a Japan Rigaku SmartLab (9kw) X-ray diffractometer. The test conditions followed the China National Petroleum and Natural Gas Industry Standard GB/T 19145-2003.[52]

3.4. Total Organic Carbon Analysis. The dried test samples were ground into particles of approximately 100 mesh in size; then, an excess of dilute hydrochloric acid solution (pure hydrochloric acid/water = 1:7) was used to dissolve the samples under constant temperature conditions of 60−80 °C for more than 2 h to remove the inorganic carbon component in the sample. Then, the samples were washed with distilled water until neutral and dried at a constant temperature of 60−80 °C; finally, the samples were combusted in a high-temperature oxygen flow (oxygen purity: 99.9%) to convert the total organic carbon into carbon dioxide, which was then detected by an infrared detector to obtain the total organic carbon content.[51,53] The experiment used a LECO CS-230 carbon-sulfur analyzer, and the test conditions followed the China National Petroleum and Natural Gas Industry Standard GB/T 19145-2003.

4. RESULTS

4.1. Outcrop Observations. The late Permian Longtan Formation of the Panguan syncline was deposited in a marine−continental transitional sedimentary environment. The Beiwujia outcrop section of the Longtan Formation, located on the southeast flank of the Panguan syncline, is well exposed due to the construction of a highway. The Longtan Formation lies on the Emeishan basalt and is covered by the
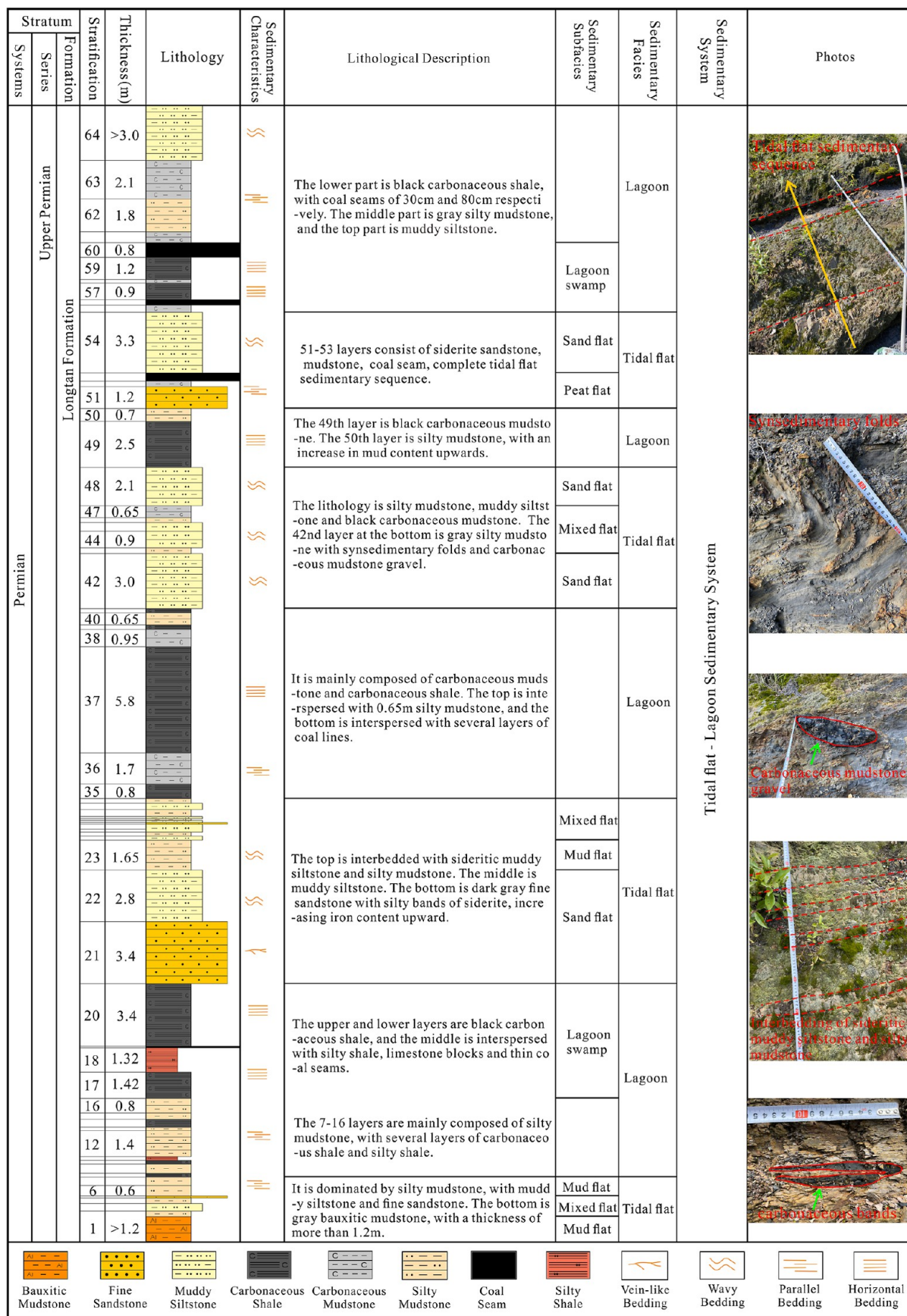
Stratum			Stratification	Thickness(m)	Lithology	Sedimentary Characteristics	Lithological Description	Sedimentary Subfacies	Sedimentary Facies	Sedimentary System	Photos
Systems	Series	Formation									

Permian / Upper Permian / Longtan Formation

Layer	Thickness	Lithological Description	Subfacies	Facies
64	>3.0	The lower part is black carbonaceous shale, with coal seams of 30cm and 80cm respectively. The middle part is gray silty mudstone, and the top part is muddy siltstone.		Lagoon
63	2.1			
62	1.8			
60	0.8			
59	1.2			Lagoon swamp
57	0.9			
54	3.3	51-53 layers consist of siderite sandstone, mudstone, coal seam, complete tidal flat sedimentary sequence.	Sand flat	Tidal flat
51	1.2		Peat flat	
50	0.7	The 49th layer is black carbonaceous mudstone. The 50th layer is silty mudstone, with an increase in mud content upwards.		Lagoon
49	2.5			
48	2.1		Sand flat	
47	0.65	The lithology is silty mudstone, muddy siltstone and black carbonaceous mudstone. The 42nd layer at the bottom is gray silty mudstone with synsedimentary folds and carbonaceous mudstone gravel.	Mixed flat	Tidal flat
44	0.9			
42	3.0		Sand flat	
40	0.65			
38	0.95			
37	5.8	It is mainly composed of carbonaceous mudstone and carbonaceous shale. The top is interspersed with 0.65m silty mudstone, and the bottom is interspersed with several layers of coal lines.		Lagoon
36	1.7			
35	0.8			
23	1.65	The top is interbedded with sideritic muddy siltstone and silty mudstone. The middle is muddy siltstone. The bottom is dark gray fine sandstone with silty bands of siderite, increasing iron content upward.	Mixed flat / Mud flat	Tidal flat
22	2.8		Sand flat	
21	3.4			
20	3.4	The upper and lower layers are black carbonaceous shale, and the middle is interspersed with silty shale, limestone blocks and thin coal seams.	Lagoon swamp	Lagoon
18	1.32			
17	1.42			
16	0.8	The 7-16 layers are mainly composed of silty mudstone, with several layers of carbonaceous shale and silty shale.		
12	1.4			
6	0.6	It is dominated by silty mudstone, with muddy siltstone and fine sandstone. The bottom is gray bauxitic mudstone, with a thickness of more than 1.2m.	Mud flat / Mixed flat / Mud flat	Tidal flat
1	>1.2			

Sedimentary System: Tidal flat - Lagoon Sedimentary System

Legend: Bauxitic Mudstone · Fine Sandstone · Muddy Siltstone · Carbonaceous Shale · Carbonaceous Mudstone · Silty Mudstone · Coal Seam · Silty Shale · Vein-like Bedding · Wavy Bedding · Parallel Bedding · Horizontal Bedding

Photo labels: Tidal flat sedimentary sequence · Synsedimentary folds · Carbonaceous mudstone gravel · Interbedding of sideritic muddy siltstone and silty mudstone · carbonaceous bands

Figure 2. Histogram of the Beiwujia outcrop section of the Longtan Formation.

Feixianguan Formation. The Beiwujia outcrop section of the Longtan Formation is approximately 62 m thick and predominantly consists of fine sandstone, muddy siltstone, silty mudstone, carbonaceous mudstone, carbonaceous shale, and coal seam (Figure 2), with yellowish-gray, dark gray, and grayish-black shale; it can be divided into 64 lithostratigraphic layers, including four layers of coal seam, 14 layers of shale, 28 layers of mudstone, and 18 layers of sandstone (Figure 3a−e).
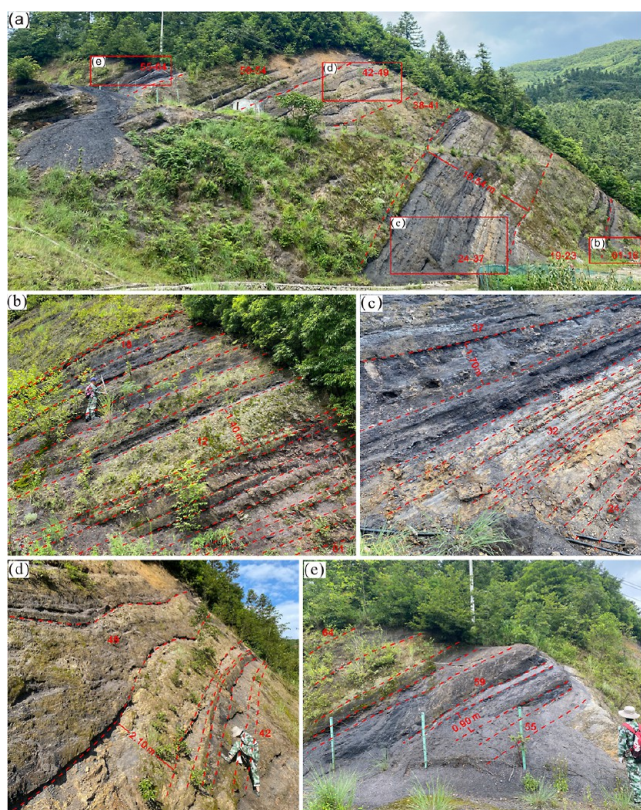

Figure 3. Stratigraphic division of the Beiwujia outcrop section. (a) Stratigraphic division of layers 1−64; (b) stratigraphic division of layers 1−18; (c) stratigraphic division of layers 24−37; (d) stratigraphic division of layers 42−49; and (e) stratigraphic division of layers 55−64.

The Longtan Formation of the section in our study area was formed in a tidal flat-lagoon depositional system. The lower section of the Longtan Formation is covered with Emeishan basalt, with a layer of gray bauxitic mudstone at the bottom, followed by muddy sandstone interbedded with thin layers of fine sandstone. The lower part of the middle section consists of sandy mudstone and black coal-bearing shale interbedded with each other and with thin coal seams. The thickness of each layer gradually increases upward, and the upper part of the middle section consists of medium to thick fine sandstone and sandy mudstone, with dark gray fine sandstone in contact with the black carbonaceous shale in an undulating pattern and siderite bands. The upper section consists of sideritic muddy sandstone and sandy mudstone interbedded with each other. The sandy mudstone is light yellow to grayish-black, with horizontal bedding. The muddy sandstone is brown, has a stable single layer with a thickness between 0.1 and 0.3 m, and is evenly distributed in the mud shale (Figure 2). The lower section of the Longtan Formation is mainly composed of lagoon and tidal flat sediments, with thin coal seams developed

in the lagoon swamp environment. Black coal-bearing shale and coal-bearing shale are developed in the lagoon sediments.

The upper section of the Longtan Formation is composed of swamp and tidal flat facies. The lower part of the upper section consists of medium-thin carbonaceous mudstone, thick carbonaceous shale, and medium-thick muddy siltstone. Wavy bedding and siderite silty bands are observed in the muddy siltstone. In the middle of the upper section, there are medium-thick fine sandstone layers interbedded with thin coal seams. The fine sandstone contains clay and is susceptible to weathering. This is followed by thick siltstone and thin coal seams. The upper part of the upper section is composed of thick carbonaceous mudstone, carbonaceous shale, and coal seam interbedded with each other and thick shale layers that contain coal seam both above and below (Figure 2). The upper section of the Longtan Formation is mainly composed of swamp and tidal flat facies, with thin coal seams developed in the swamp and peat flat facies and dark-colored carbonaceous mudstone and carbonaceous shale developed in the lagoon facies.

4.2. Total Organic Matter Content. The total organic matter content (TOC) is one of the most important indicators for evaluating shale gas reservoirs. Table 1 lists the TOC values of 14 Longtan Formation samples from the MY101 well in the study area. The TOC values of the Longtan Formation samples are generally high, ranging from 1.44 to 14.79%, with an average of 6.41%. Approximately 78.6% of the Longtan Formation samples have TOC values exceeding 2% (Figure 5), indicating that most samples have good potential for shale gas resources. The TOC of the Longtan Formation varies significantly in the vertical direction, with a general trend of initially increasing and then decreasing from bottom to top (Figure 2). The Longtan Formation has major differences in the lithology in the vertical direction, with various lithologies such as mudstone, coal seam, and siltstone alternating, resulting in significant changes in TOC in the vertical direction; the sedimentary environment shows significant changes during the deposition of the Longtan Formation and has different lithologic characteristics. The TOC content of the strata near the coal seam is very high,[54−57] ranging from 10 to 15% (Figure 2).

4.3. Maceral and Organic Matter Type. The organic macerals of the Longtan Formation in the study area are mainly composed of vitrinite, accounting for approximately 80% of the total. The vitrinite in the samples is mainly collinite, including telocollinite and desmocollinite (Figure 6c,d), with some samples containing telinite and a small amount of vitrodetrinite (Figure 6a,b). In addition, there is a small amount of inertinite, including fusinite, semifusinite, and macrinite, with fusinite exhibiting bright yellow or white reflectance and semifusinite exhibiting a slightly lower reflectance with a grayish color (Figure 6e−g). Some samples contain a small amount of bituminite (Figure 6h). The type index (TI) values are obtained based on the organic maceral composition data for the determination of the kerogen type. TI values less than 0 indicate type III kerogen, TI values between 0 and 40 indicate type II$_2$ kerogen, TI values between 40 and 80 indicate type II$_1$ kerogen, and TI values greater than 80 indicate type I kerogen.[58,59] According to statistical analysis (Table 2) and the data statistics from other studies (Table 3), type III kerogen is mainly present in the Longtan Formation in the study area, with the organic matter predominantly derived from terrigenous higher plants. The organic macerals of the

Table 1. Mineral Composition of the Longtan Formation Sample in the Study Area[a]

sample no	lithofacies	depth (m)	kaolinite (%)	I/S (%)	quartz (%)	feldspar (%)	dolomite (%)	calcite (%)	siderite (%)	pyrite (%)	anatase (%)
MY101-01	silty mudstone	432.1	3	37	15	20	17	/	/	5	3
MY101-02	carbonaceous shale	442.3	13	41	20	9	1	/	8	1	7
MY101-03	carbonaceous mudstone	464.8	3	31	21	24	12	/	/	6	3
MY101-04	bioclastic-bearing sandstone	471.8	/	31	37	7	22	/	/	1	2
MY101-05	carbonaceous shale	474.1	/	58	15	11	/	/	/	10	6
MY101-06	muddy siltstone	488.8	/	/	73	/	7	/	/	12	8
MY101-07	carbonaceous shale	510.0	4	43	25	15	3	/	5	2	3
MY101-08	carbonaceous mudstone	543.3	2	34	22	38	/	/	/	1	3
MY101-09	carbonaceous shale	561.1	72	/	17	/	/	/	/	3	8
MY101-10	carbonaceous shale	572.1	/	34	26	37	/	/	/	1	2
MY101-11	silty mudstone	590.0	/	37	24	30	6	/	/	/	3
MY101-12	carbonaceous mudstone	611.5	/	26	60	6	/	/	/	7	1
MY101-13	carbonaceous mudstone	624.3	/	22	65	/	7	/	/	5	1
MY101-14	carbonaceous mudstone	627.3	2	58	33	/	/	/	/	5	2
MY101-15	bioclastic-bearing mudstone	630.7	/	20	52	/	8	14	/	5	1
MY101-16	bioclastic-bearing mudstone	635.0	79	/	1	9	/	/	6	/	5

[a]I/S is the mixed layer of illite/smectite; "/" means no data.

Longtan Formation in the study area greatly vary in the vertical direction, with vitrinite being the dominant component, accounting for over 60% of the total. The proportion of vitrinite from bottom to top initially increases and then decreases in the formation. The inertinite component is the second highest, with a content ranging from 2.31 to 40.57%, and is primarily distributed between 20 and 30%. The proportion of inertinite initially increases and then decreases from the bottom to the top of the formation. The content of exinite is very low and that of sapropelite is the lowest. The variation in organic macerals in the Longtan Formation in the vertical direction shows significant changes in sedimentary environments during the deposition of the Longtan Formation, and the organic matter is mainly derived from terrigenous higher plants. Overall, the Longtan Formation in western Guizhou is type III and gas-prone source rock.

4.4. Mineralogical Composition. The mineral composition of shale reflects its sedimentary environment and diagenetic evolution.[10,60,61] The mineral composition consists of clay minerals, brittle minerals (including quartz, plagioclase, and pyrite), and carbonate minerals (including calcite, dolomite, and siderite).[11] As shown in Table 1, the mineral composition of the Longtan Formation in the study area is dominated by clay minerals (average 40.63%), which are predominantly composed of kaolinite (average 11.13%) and illite/smectite mixed layers (average 26.69%). The proportions of illite and chlorite are very low and can be disregarded. The next most abundant minerals are quartz (average 31.63%) and feldspar (average 12.88%). Other minerals, such as calcite, dolomite, pyrite, siderite, and anatase, can also be observed in some samples, with average contents of less than 6.00%. The ternary diagram of the mineral composition of Longtan Formation samples in the study area (Figure 7) shows the relative proportions of clay minerals, carbonate minerals, and quartz/feldspar. More than 80% of Longtan Formation samples are located in the right area, indicating that the basic mineral composition of the marine−continental transitional facies contains relatively rich clay minerals and brittle minerals but low carbonate minerals. The mineral content of

the Longtan Formation considerably varies in the vertical direction (Figure 4), and the proportion of clay minerals changes from bottom to top with a downward trend followed by an upward trend. The trend of quartz changes from bottom to top with an upward trend followed by a downward trend, and the content of feldspar was not found in some samples. The lithofacies of the Longtan Formation greatly varies in the vertical direction, with various lithofacies such as mudstone, coal seam, and siltstone appearing alternately, resulting in a large variation in the mineral composition proportion in the vertical direction and showing significant changes in the sedimentary environment and the formation of different lithofacies and mineral compositions.

4.5. Lithofacies Characteristics. Lithofacies represent a certain sedimentary environment and are used to characterize the lithological and sedimentary features of sedimentary rocks, including rock color, stratification, texture, particle size, mineral compositions, and so on.[62−65] Generally, the lithofacies of sedimentary rocks are described and distinguished through qualitative and quantitative parameters such as color, grain size, mineral composition, primary sedimentary structures, deformation structures, and biological disturbances.[66] By observing the lithology, sedimentary structures, and photomicrographs of the MY101 well core, eight typical lithofacies types were identified in the Longtan Formation of the study area of western Guizhou; these include silty mudstone, muddy siltstone, carbonaceous mudstone, carbonaceous shale, bioclastic-bearing mudstone, bioclastic-bearing siltstone, fine sandstone, and coal seam, of which the first six are fine-grained sedimentary rocks.

4.5.1. Silty Mudstone. The lithofacies color of silty mudstone is gray to dark gray, with a pelitic texture, wavy bedding, and horizontal bedding (Figure 9a), and the silty mudstone has a main mineral composition of clay minerals, sandy debris, and dolomite, with a small amount of pyrite. The clay mineral content is relatively large, at an average of 38.5%, and appears as microscopic flakes. Quartz and feldspar are the main components of the sandy debris, with average contents of 19.5 and 25%, respectively, showing a subcircular single-crystal
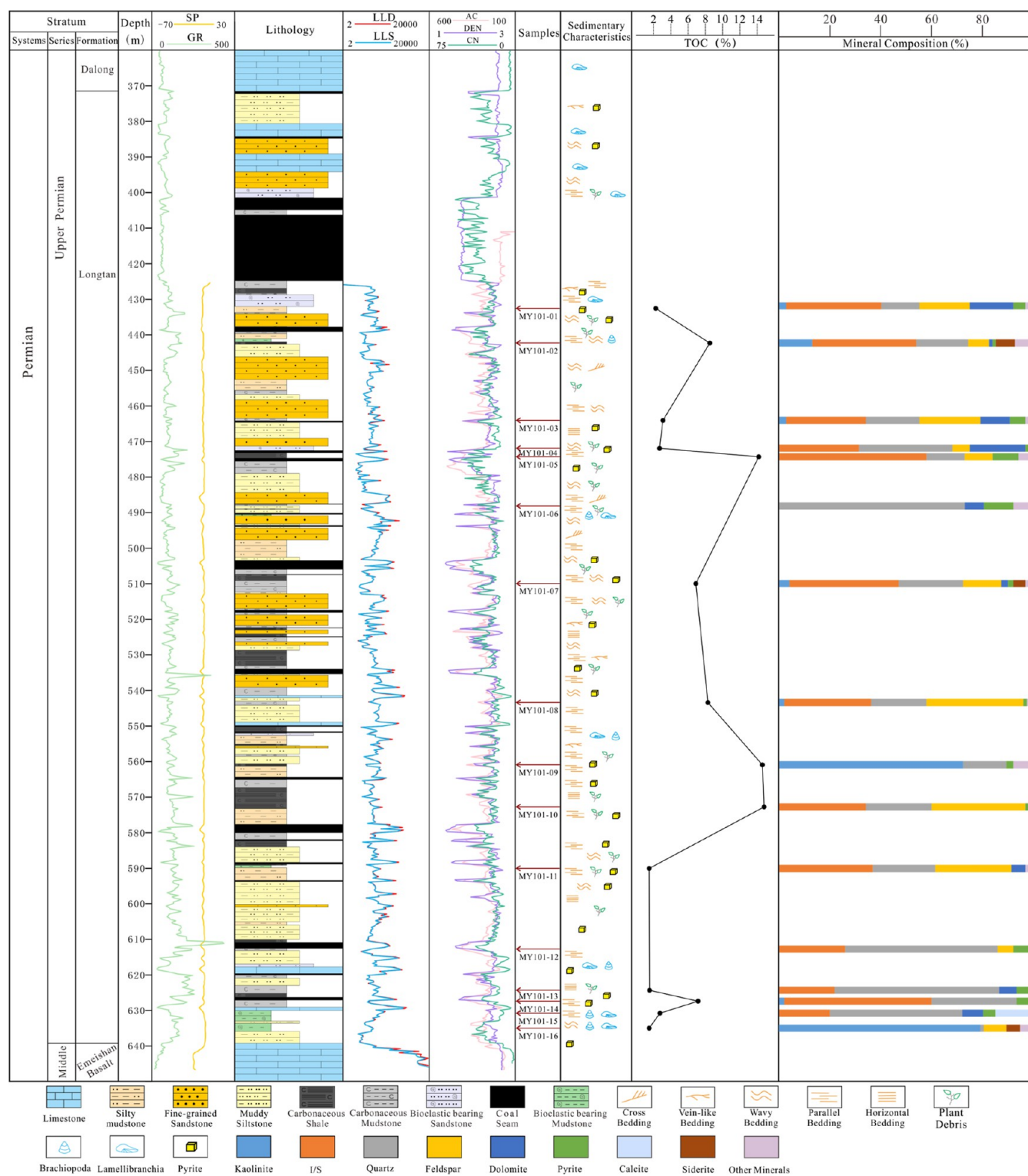
Figure 4. Comprehensive histogram of the MY101 well.

distribution. The average dolomite content is 11.5%, and the average pyrite content is 3%. The organic matter of the silty mudstone has a diffused distribution in microscopic form (Figure 8a,b), and the TOC content is general, with an average of 1.89%. The maceral components of this lithofacies are mainly vitrinite and inertinite with average contents of 48.02 and 45.66%, respectively, and a small amount of liptinite with

an average content of 6.32%. The kerogen TI ranges from −80.84 to −76.19, corresponding to a type III kerogen.

4.5.2. Muddy Siltstone. The lithofacies of muddy siltstone is gray in color overall with wavy bedding and horizontal bedding (Figure 9b). Macroscopically, it is composed of thin silty sand and mudstone interbedding. The silty content is 30−40%, the color is gray, and horizontal bedding is developed. Microscopically, the main minerals are sandy clasts, followed by
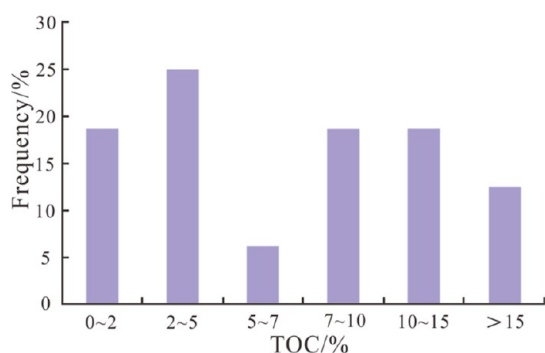
Figure 5. Distribution map of the TOC in samples from the Longtan Formation in the study area.

dolomite and pyrite. The sandy debris is mainly quartz, with a content of 73%. The sandy debris is distributed in strips and clay mineral microlayers. The organic matter of the muddy siltstone has a discrete distribution in the microscopic form, and the TOC content is 3.18% (Figure 8c,d).

4.5.3. Carbonaceous Mudstone. The lithofacies of carbonaceous mudstone as a whole is a gray-black to black, mostly massive structure (Figure 9e); the lithofacies and coal seam often appear at the same time and are generally observed in the upper and lower parts of the coal seam. Some samples contain thin coal lines and plant fossils (Figure 9c,d). The carbonaceous mudstone is dominated by clay minerals and quartz with average contents of 35.6 and 40.2%, respectively. The clay minerals are in a directional arrangement (Figure 8f), the

feldspar content is low with an average content of 13.6%, and a small amount of pyrite with an average content of 4.8% is present. The carbonaceous mudstone has a higher organic matter content (Figure 8e,g), with a stratified and banded distribution in the microscopic form, and a higher TOC content with an average of 5.0%. The maceral components of this lithofacies are mainly vitrinite and inertinite with average contents of 63.64 and 26.48%, respectively, and small amounts of liptinite and sapropelite with average contents of 9.42 and 0.46%, respectively. TI ranges from −77.04 to −60.19, corresponding to a type III kerogen.

4.5.4. Carbonaceous Shale. The lithofacies of carbonaceous shale is overall black in macroscopic appearance, leaving no stains on hands, with developed bedding planes. Some samples contain pyrite, which is centimeter massive or banded, occasionally interspersed with calcite veins, and contains plant fossils (Figure 9f,g). The main mineral is clay, with an average content of approximately 53%, and appears as microscopic flakes arranged in a directional manner to form bedding plane-like structures (Figure 8h,i). It contains a small amount of sandy debris and gravel debris, composed of quartz and feldspar, in the form of a subcircular single-crystal distribution, with average contents of 20.6 and 14.4%, respectively. The pyrite content is very low, with an average content of 4.8%. The carbonaceous shale has a high content of organic matter and is stratified and banded in microscopic form. Among the six fine-grained lithofacies, the TOC content of carbonaceous shale is the highest, with an average of 11.8%. The maceral components of this lithofacies are mainly vitrinite and inertinite with average contents of 59.69 and 30.56%,
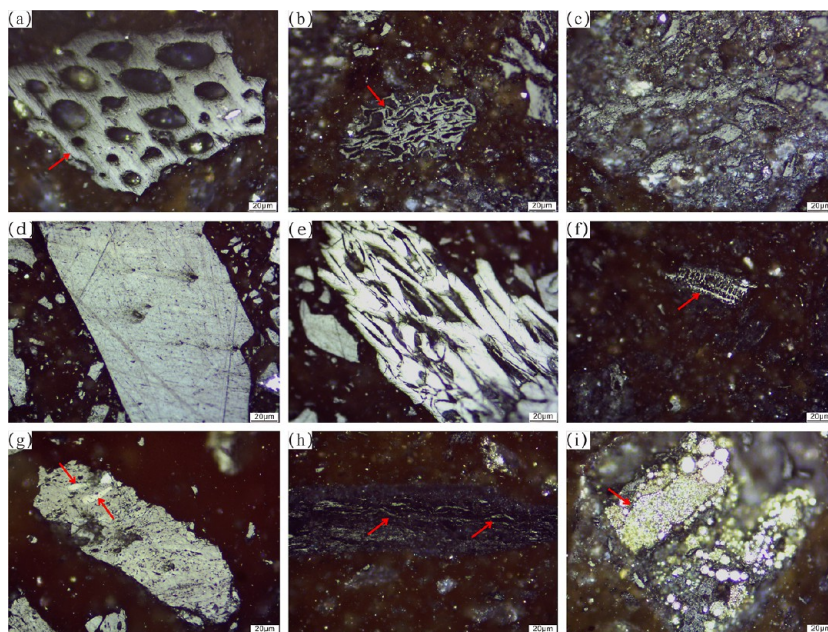

Figure 6. Longtan Formation samples of the MY101 well photographed under oil immersion, reflected white light conditions, showing the organic macerals and pyrite. (a) Telinite 1, with relatively intact cell cavities and appearing light gray, sample location: 373.6 m. (b) Telinite 2, with strong expansion of the plant cell wall and deformation of the cell cavity, appearing light gray, sample location: 561.1 m. (c) Desmocollinite, without a fixed shape and no traces of cell structure, appearing light gray, sample location: 474.0 m. (d) Telocollinite, strip-like, with uniform internal structure and developed original cracks, appearing gray, sample location: 488.7 m. (e) Fusinite, with clear intercellular spaces and vessel pits, appearing bright white, sample location: 488.7 m. (f) Semifusinite, with poor preservation of cell structure and slightly lower elevation, appearing light gray, but compared to fusinite, it has a grayish tint, sample location: 572.0 m. (g) Macrinite, appearing strip-like, with desmocollinite distributed around its periphery, appearing light white, sample location: 400.6 m. (h) Bituminite, appearing as thin strip-like structures and in a gray-black color, sample location: 627.2 m. (i) Pyrite, gathered in strawberry-like clusters and distributed around the vitrinite, sample location: 439.2 m.

Table 2. TOC Content and Maceral Composition of the Longtan Formation, the MY101 Well[a]

sample no	TOC (%)	sapropelite	exinite	vitrinite	inertinite	TI	kerogen type
MY101-01	2.27	/	/	95.24	4.76	−76.19	III
MY101-02	8.52	/	6.97	81.04	11.99	−69.28	III
MY101-03	3.09	/	4.76	63.28	31.96	−77.04	III
MY101-04	2.69	0.88	0.5	93.36	5.26	−74.15	III
MY101-05	14.18	0.42	2.33	88.81	8.44	−73.46	III
MY101-07	6.90	1.38	5.92	85.32	7.38	−67.03	III
MY101-08	8.31	0.98	11.03	85.23	2.76	−60.19	III
MY101-09	14.58	0.23	12.71	17.54	69.52	−76.09	III
MY101-10	14.79	2.14	16.67	25.74	55.45	−64.28	III
MY101-11	1.50	/	12.64	0.79	86.57	−80.84	III
MY101-13	1.55	/	9.28	88.51	2.21	−63.95	III
MY101-14	7.15	0.86	12.63	17.52	68.99	−74.96	III
MY101-15	2.74	4.05	9.45	8.55	77.95	−75.59	III
MY101-16	1.44	21.21	17.3	61.49	/	−16.26	III

[a]TI = type index = 100 × (sapropelite, %) + 50 × exinite, %) − 75 × (vitrinite, %) − 100 × (inertinite, %); "/" means no data.

Table 3. Maceral Composition Data of the Longtan Formation in the Study Area[a]

area	lithofacies	sapropelite	exinite	vitrinite	inertinite	data source
Chishui, Northern Guizhou	black shale	0.22	2.53	$\frac{59.00 \sim 97.20}{85.50}$	11.75	Cao et al., 2018
Eastern of Panxian	black shale	$\frac{2 \sim 18}{7.8}$	$\frac{5 \sim 46}{21.4}$	$\frac{27 \sim 89}{63.3}$	$\frac{2 \sim 15}{7.5}$	Deng et al., 2020
Jinsha, Northern Guizhou	black shale		$\frac{7 \sim 29}{16.5}$	$\frac{28 \sim 81}{52.3}$	$\frac{13 \sim 55}{31.2}$	Deng et al., 2020
Xiashi Town,Majiang	black shale		$\frac{0 \sim 14.29}{5.42}$	$\frac{85.71 \sim 97.87}{93.19}$	$\frac{0 \sim 5.56}{1.39}$	Wang et al., 2012
Northwest of Qianxi	black shale		$\frac{18 \sim 59}{36}$	$\frac{8 \sim 43}{23.5}$	$\frac{20 \sim 75}{23.5}$	Luo et al., 2018
Southeast of Panxian	black shale	$\frac{0 \sim 4.05}{0.84}$	$\frac{0 \sim 16.67}{8.07}$	$\frac{0.79 \sim 95.24}{57.76}$	$\frac{2.21 \sim 86.57}{33.33}$	experimental data

[a]Note: the meaning of the numbers in the table is as follows: $\frac{(minimum\ value\ \sim\ maximum\ value)}{average\ value}$.
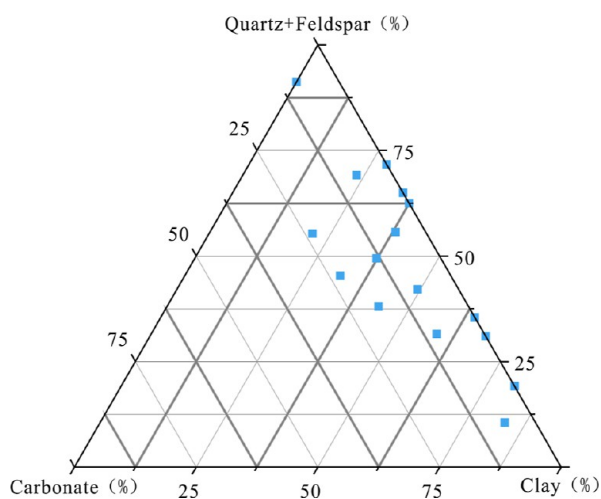

Figure 7. Ternary diagram of the mineral composition of the Longtan Formation in the study area.

respectively, and small amounts of exinite and sapropelite with average contents of 8.92 and 0.83%, respectively. The TI ranges from −76.09 to −64.28, corresponding to a type III kerogen.

4.5.5. Bioclastic-Bearing Mudstone. The lithofacies of bioclastic-bearing mudstone is gray-dark gray, with a pelitic

texture and no evident bedding. It contains a large number of bioclasts (Figure 9h), some of which are partially diagenetically altered or silicified; their original shape is preserved and includes circular, univalve, or irregular shapes. Bioclastic-bearing mudstone is mainly composed of bioclasts, such as brachiopods, ostracods, and other organisms (Figure 8j,k). Its main mineral compositions are clay minerals, sandy debris, and calcite, with a small amount of dolomite and pyrite. The average clay mineral content is 49.5% and appears as microscopic flakes. The average content of sandy debris is approximately 30%. It is mainly composed of quartz with an average content of 26.5% and a small amount of feldspar with an average content of 4.5%. The average content of calcite is 7%, and the average contents of dolomite and pyrite are 4 and 2.5%, respectively. The organic matter of bioclastic-bearing mudstone is diffusely distributed in the microscopic form, and the TOC content is general, with an average of 2.09%. The maceral components of this lithofacies are mainly vitrinite and inertinite, with average contents of 35.02 and 38.98%, respectively, while the contents of exinite and sapropelite are general, with average contents of 13.37 and 12.63%, respectively. The TI ranges from −75.59 to −16.26, corresponding to a type III kerogen.

4.5.6. Bioclastic-Bearing Sandstone. The lithofacies of bioclastic-bearing sandstone is gray-dark gray, with a pelitic texture and no evident bedding (Figure 9i). It contains a large
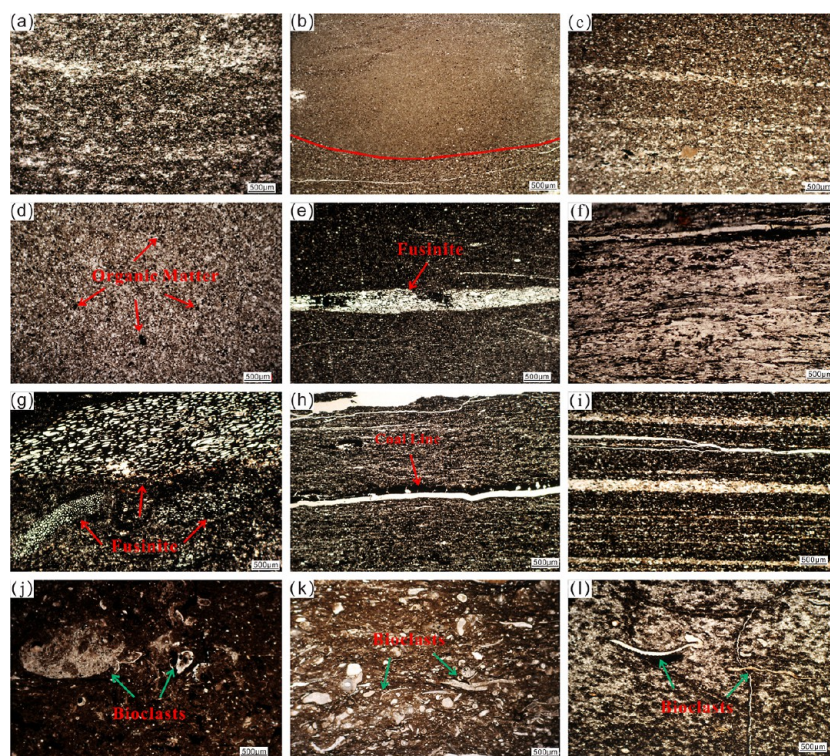
Figure 8. Thin sections showing the typical fine-grained lithofacies of the Permian Longtan Formation in the western Guizhou region. (a) Silty mudstone, with directional distribution of mineral particles and dispersed distribution of black organic matter, 558.5 m from the MY101 well; (b) silty mudstone, contact line between mud and silt, 488.8 m from the MY101 well; (c) muddy siltstone, horizontal bedding, discrete distribution of black organic matter, 458.1 m from the MY101 well; (d) muddy siltstone, discrete distribution of black organic matter, 584.5 m from the MY101 well; (e) carbonaceous mudstone, with fusinite, 611.5 m from the MY101 well; (f) carbonaceous mudstone, directional arrangement of clay minerals and black organic matter, 627.3 m from the MY101 well; (g) carbonaceous mudstone, developed filamentous bodies, Xiaozhaicun section; (h) carbonaceous shale, black organic matter and clay minerals arranged in a directional manner, with well-developed coal lines, 474.1 m from MY101 well; (i) carbonaceous shale, horizontal bedding, layered distribution of black organic matter, 510.0 m from the MY101 well; (j) bioclastic-bearing mudstone, 630.7 m from the MY101 well; (k) bioclastic-bearing mudstone, Zuojiazhai section; and (l) bioclastic-bearing siltstone, 400.7 m from the MY101 well.

number of bioclasts (Figure 8l), some of which are partially diagenetically altered or silicified; their original shape is preserved and includes circular, univalve, or irregular shapes. Bioclastic-bearing sandstone is mainly composed of bioclasts, such as brachiopods, ostracods, and other organisms. Its main mineral compositions are sandy debris, clay minerals, dolomite, and a small amount of pyrite. The content of sandy debris is approximately 48%, and the composition is mostly quartz, with a content of 37%, and a small amount of feldspar, with a content of 7%. The dolomite content is 22%. The clay mineral content is 31% and appears as microscopic flakes. The pyrite content is very low at only 1%. The organic matter in bioclastic sandstone has a dispersed distribution in the microscopic form, and the TOC content is generally 2.69%. The macerals of this lithofacies are mainly vitrinite at 93.36% and small amounts of inertinite, exinite, and sapropelite at 5.26, 0.5, and 0.88%, respectively. The TI value is −74.15, corresponding to a type III kerogen.

4.5.7. Fine Sandstone. The lithofacies of fine sandstone is grayish-white and thin to medium bedded, with intercalated bedding, parallel bedding, and ripple bedding; it is generally poorly sorted, with low roundness and mostly subangular in shape. Fine sandstone is a short-distance transport product primarily composed of quartz with a certain amount of other lithic fragments and minor amounts of feldspar. The matrix minerals are clay minerals. Locally, there are black ribbon-like

and lump-like mudstones, and pyrite nodules can be found in some fine sandstones of the upper part of the Longtan Formation.

4.5.8. Coal Seam. The lithofacies of the coal seam is black, stains the hand, has a massive structure, and has a metallic luster, and pyrite nodules can be locally found. Scratch marks and sliding surfaces are observed. The coal seam is formed by the accumulation of plant debris and peat.

5. DISCUSSION

5.1. Organic Matter Input. Different types of organic matter are derived from different types of primary production, such as algae or terrigenous higher plants.[67] Furthermore, the compositional characteristics of kerogen can provide insights into the changes in the sedimentary environment and the sources of organic matter during the sedimentation process.[68−70] Organic matter types not only determine the type of hydrocarbons generated from shale but also affect the pathways of hydrocarbon evolution.[29,71] The comprehensive identification of organic macerals (Table 2) shows that the Longtan Formation in this region is mainly composed of type III kerogen, and the organic matter predominantly comes from the input of terrigenous higher plants. Therefore, during the entire stage of maturation and evolution, the generated hydrocarbons are mainly gaseous.
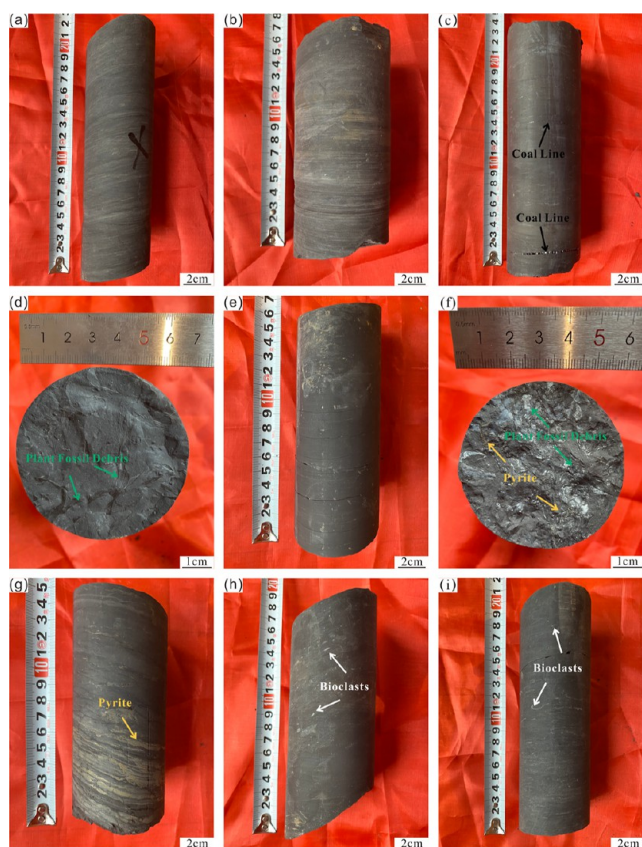
Figure 9. Core samples from the MY101 well of typical fine-grained lithofacies of the Permian Longtan Formation in the western Guizhou region. (a) Silty mudstone, dark gray, horizontal bedding, sample location: 432.4 m; (b) muddy siltstone, gray, horizontal bedding, sample location: 564.1 m; (c) carbonaceous mudstone, dark gray, coal-bearing line (black arrow), sample location: 611.5 m; (d) carbonaceous mudstone, gray-black, plant fossil debris (green arrow), sample location: 525.4 m; (e) carbonaceous mudstone, gray-black, massive structure, sample location: 442.3 m; (f) carbonaceous shale, black, plant fossil debris (green arrow), pyrite particles (yellow arrow), sample location: 594.2 m; (g) carbonaceous shale, gray-black, pyrite-layered distribution (yellow arrow), sample location: 465.0 m; (h) bioclastic-bearing mudstone, dark gray, bioclasts (white arrow), sample location: 630.7 m; and (i) bioclastic-bearing siltstone, dark gray, bioclasts (white arrow), sample location: 471.8 m.

The relationship between TOC and clay minerals and quartz is shown in Figure 10. The TOC content increases with increasing clay mineral content; there is a positive correlation between TOC and clay minerals, while there is no significant correlation between TOC and quartz. Our result contradicts the results from previous studies on marine shale, where there was a positive correlation between TOC and quartz,[42] and a negative correlation between TOC and clay minerals.[72] Previous studies have shown that these differences can be related to different sedimentary environments.[52,73] The increase in quartz content with increasing TOC in shale indicates its biogenic origin.[10,65,73−75] Figure 10 shows that most samples in the Longtan Formation of the study area are not of biogenic origin, differing from the conclusions drawn from the marine shales of the Niutitang Formation and Longmaxi Formation. The Longtan Formation in the western Guizhou region is a marine−continental transitional sedimentary environment of a lagoon-tidal flat and delta sedimentary facies. Therefore, the ancient Kangding-Yunnan land to the west of the study area is the main source area for sediment in the late Permian of Guizhou, and it has an important control on the sedimentation in the region.

5.2. Lithofacies Assemblages. A lithofacies assemblage refers to a set of symbiotic lithofacies that are closely related in terms of their genesis and sedimentary environment.[76,77] A lithofacies assemblage reflects a certain sedimentary environment and its sedimentary processes and is a product of a single sedimentary event or a continuous evolution of a specific environment. Lithofacies assemblages represent specific environmental conditions during a particular period, such as climate, hydrodynamics, and sediment sources, and can reflect the regular evolution of each environmental condition.[78,79] Based on observations of the core samples and thin sections in the study area and combined with the analysis of measurement and logging data, the six typical lithofacies assemblages are believed to have mainly developed in the Longtan Formation in western Guizhou. Typical core segments and field sections were selected to describe the developmental patterns and petrological characteristics of the lithofacies in the six lithofacies assemblages (Table 4).

5.2.1. Lithofacies Assemblage A. The lithofacies assemblage A is composed of muddy sandstone and sandy mudstone, which alternate in a layered distribution. The thicknesses of the muddy sandstone and sandy mudstone are relatively small, and they are thinly layered with horizontal bedding, with some
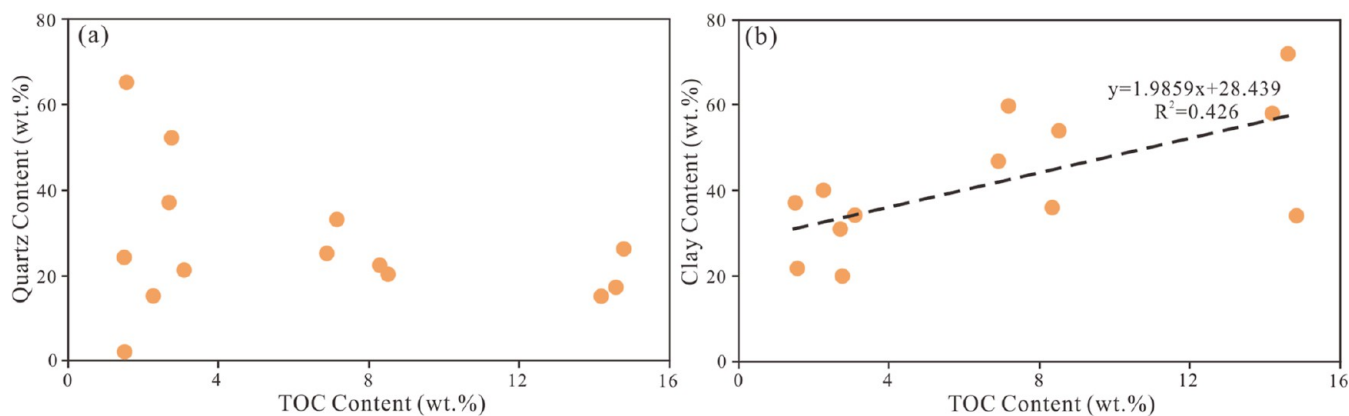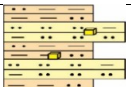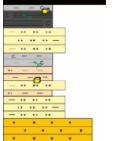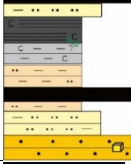

Figure 10. Relationships between TOC content and quartz content (a) and clay content (b) of transitional Longtan samples from the study area.

Table 4. Lithofacies Assemblage of the Longtan Formation in the Study Area

NO.	Illustration	Lithofacies Assemblage	Description	Sedimentary Environment
A		Muddy sandstone + sandy mudstone	The two lithofacies alternate in a layered distribution, and they are thinly layered with horizontal bedding, and some contain pyrite nodules.	Lagoon
B		Coal seam+carbonaceous mudstone+ carbonaceous shale	The coal seams and black shale are alternately developed in a thin layer with horizontal bedding and wavy bedding and contain plant debris fossils and pyrite nodules.	Peat swamp
C		Silty mudstone+carbonaceous mudstone+carbonaceous shale+coal seam	Carbonaceous shale and carbonaceous mudstone are relatively thick, containing biological fossils and plant debris fossils, and the pyrite is developed.	Lagoon
D		Fine sandstone+muddy siltstone+silty mudstone+carbonaceous mudstone+carbonaceous shale+coal seam	The lithology of peat flat is composed of coal seams, silty mudstone, carbonaceous mudstone, and carbonaceous shale; the mixed flat deposit is composed of muddy siltstone, silty mudstone and carbonaceous mudstone; the fine sandstone and argillaceous siltstone are sand flat.	Tidal flat peat flat -mixed flat-sand flat
E		Fine sandstone+silty mudstone+muddy siltstone+carbonaceous mudstone+carbonaceous shale+coal seam	Fine sandstone is thick bedded and the pyrite is developed; silty mudstone and muddy siltstone are the main body of the distributary bay, with thin layers of carbonaceous mudstone, carbonaceous shale and coal seam. Horizontal bedding and vein-like bedding are developed, and plant debris fossils are produced.	River mouth bar-interdistributary bay
F		Fine sandstone+ coal seam	The bottom of this lithofacies assemblage is a thick layered fine sandstone and the upward lithology suddenly changes into a thin layer of coal.	Delta plain

containing pyrite nodules. This lithofacies assemblage is formed by fine-grained sediment and is a characteristic feature of lagoon environments, indicating the relatively quiet water environment characteristics of the lagoon facies.

5.2.2. Lithofacies Assemblage B. The lithofacies assemblage B is composed of coal seams, carbonaceous mudstone, and carbonaceous shale. The coal seam and black shale alternate to form a black coal-bearing stratum. Carbonaceous mudstone and carbonaceous shale are thinly layered with horizontal and ripple bedding and contain plant debris fossils and pyrite nodules. Carbonaceous mudstone and carbonaceous shale have high organic matter contents and are typical organic-rich mudstones and shale. The coal seam is mostly a thin to medium-thick layer containing pyrite nodules, indicating frequent changes in the aquatic environment at that time. This type of lithofacies assemblage indicates peat swamp facies.

5.2.3. Lithofacies Assemblage C. The lithofacies assemblage C is composed of siltstone, carbonaceous mudstone, carbonaceous shale, and coal seam, occurring in thin layers with horizontal and vein-like bedding planes. The thickness of carbonaceous shale and carbonaceous mudstone is thick, containing fossils and plant clastic fossils, and the pyrite is developed. This assemblage primarily represents sedimentation in the lagoon environment with weak hydrodynamics.

5.2.4. Lithofacies Assemblage D. The lithofacies assemblage D is composed of fine sandstone, muddy siltstone, silty mudstone, carbonaceous mudstone, carbonaceous shale, and coal seam, forming a sedimentary sequence of peat flat-mixed flat-sand flat. The peat flat deposition is composed of coal seams, siltstone, carbonaceous mudstone, and carbonaceous shale. The mudstone is dark gray, and the siltstone is gray, occurring in thin layers with horizontal bedding and ripple bedding and containing pyrite nodules and plant debris fossils. The mixed flat deposition is composed of interbedded muddy siltstone, silty mudstone, carbonaceous mudstone, and carbonaceous shale, occurring in thin layers with horizontal bedding and ripple bedding and containing pyrite nodules and plant debris fossils. The fine sandstone and muddy sandstone represent the sand flat deposition, occurring in thin- to medium-thickness layers with cross-bedding and ripple-bedding planes. Silty mudstone, carbonaceous mudstone, and carbonaceous shale are organic-rich lithofacies with high organic carbon contents but low thicknesses. This assemblage represents fine-grained sedimentation and indicates a tidal flat facies peat flat-mixed flat-sand flat sedimentary environment.

5.2.5. Lithofacies Assemblage E. The lithofacies assemblage E is composed of fine sandstone, silty mudstone, muddy siltstone, carbonaceous mudstone, carbonaceous shale, and coal seam. The thick-bedded fine sandstone has vein-like bedding and cross-bedding with black muddy bands containing siderite nodules and pyrite mineralization, indicating a river mouth bar sedimentary environment. The thin-bedded silty mudstone and muddy siltstone form the main body of the interdistributary bays; these bays are interspersed with thin layers of carbonaceous mudstone, carbonaceous shale, and coal seam; occur with horizontal and vein-like bedding; and contain plant debris fossils and high organic carbon content. This assemblage indicates a river mouth bar-interdistributary bay sedimentary environment at the front of the delta.

5.2.6. Lithofacies Assemblage F. The lithofacies assemblage F is composed of fine sandstone and coal seam. The bottom of the assemblage is thick layered fine sandstone, with developed cross-bedding and vein-like bedding. The upper lithology suddenly changes into a thin layer of coal. The thick fine sandstone in the lower part represents river channel deposition, while the coal seam is mainly developed in the swamp environment formed by river channel deposits. This
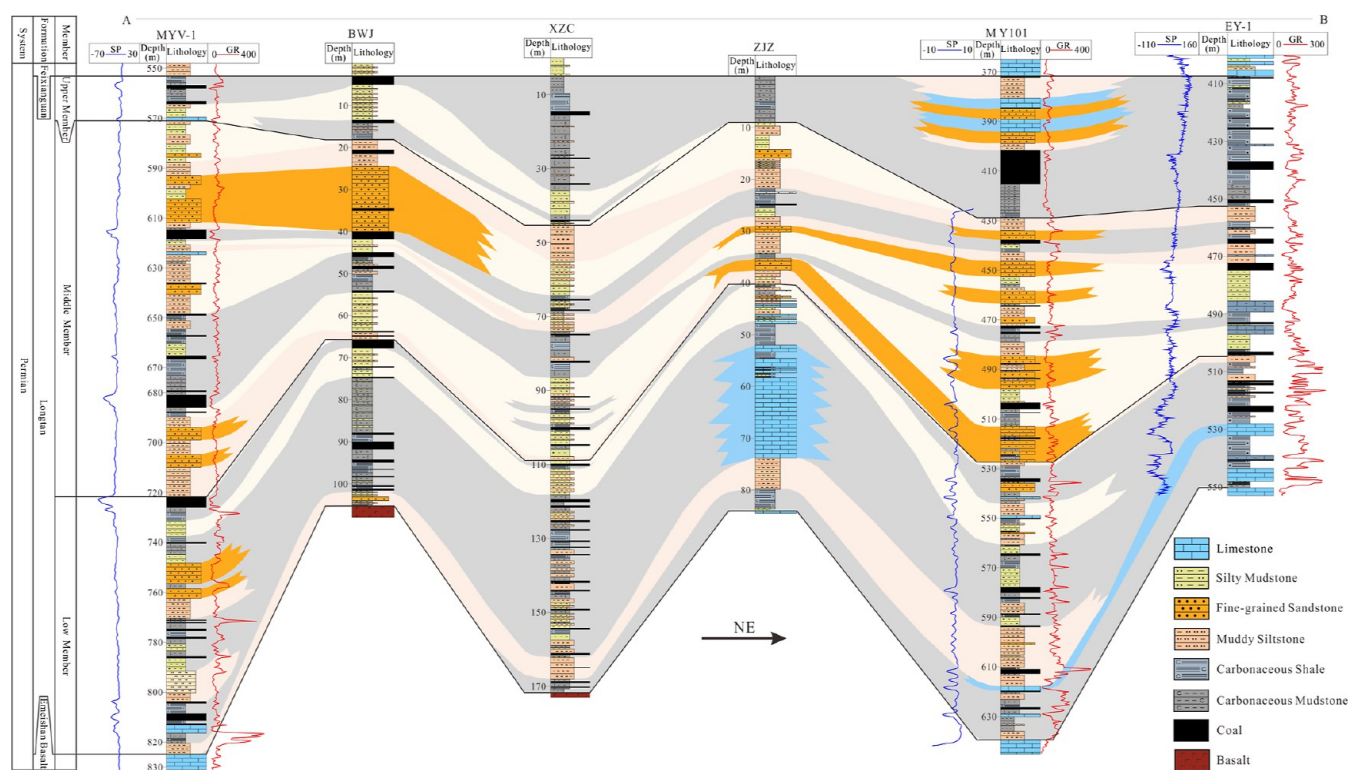
Figure 11. Cross section of the well connection in the study area (section location seen in Figure 1b).

assemblage primarily represents the delta plain sedimentary environment.

5.3. Sedimentary Model. *5.3.1. Sedimentary Facies Distribution.* Based on the analysis of the lateral distribution characteristics of lithofacies in the Longtan Formation in the western Guizhou area using the southwest−northeast well-to-well correlation profile (Figure 1b), the results show that there are significant differences in lithofacies distribution in the study area (Figure 11). According to the lithofacies assemblage and the vertical lithofacies variation, the Longtan Formation is divided into three sections.

The lower section of the Longtan Formation in the study area has complex and diverse lithofacies, mainly consisting of muddy sandstone, sandy mudstone, carbonaceous mudstone, and carbonaceous shale, with multiple thin coal seams. The lithofacies change rapidly in the vertical direction, and the lithofacies thickness is relatively thin, indicating that the sedimentary environment quickly changed. In the southern part of the study area, there are thin layers of carbonate at the bottom of the lower section, and thicker layers of fine sandstones develop at the top of the lower section. From southwest to northeast, the thickness of the lithofacies becomes thinner, and mud and sand are interbedded. In the central part of the study area, a layer of approximately 20 m-thick carbonate rock is developed in the lower section. In the northern part of the study area, a thin layer of carbonate rock is developed at the bottom and middle of the lower section.

The middle section of the Longtan Formation in the study area is mainly composed of muddy sandstone, carbonaceous mudstone, and carbonaceous shale, with multiple thin coal seams. The sandy mudstone is thin and interbedded with muddy sandstone. In the southern part of the study area, muddy siltstone at the bottom and the top of the middle section is interspersed with thick fine sandstone, which is

pinched out along the northeast direction. In the central part of the study area, thin layers of fine sandstone are developed, interbedded with muddy sandstone, pinched out along the northeast direction, and extended to the northern part of the study area.

The upper segment of the Longtan Formation in the study area is mainly composed of carbonaceous mudstone and sandy mudstone, with a thin coal seam. In the southern and central parts of the study area, sandy mudstone and muddy sandstone are interbedded in thin layers. In the northern part of the study area, thick layers of muddy sandstone, carbonate, and fine sandstone are developed and pinched out along the northeast and southwest directions.

5.3.2. Depositional Model. Based on the lithofacies assemblage types, lithofacies distribution, and organic microfacies variation, a sedimentary model for the study area is established. The sedimentary environment in western Guizhou has undergone significant changes, with multiple small-scale transgressions and continuous regressions occurring from the Carboniferous to the Permian.[47] In the middle of the Permian, the study area had a paleogeographic pattern of high northwest and low southeast. The Dongwu movement caused crustal uplift in South China and the large-scale eruption of the Emeishan basalt. The ancient continent that had significant control on sedimentation in the area was the ancient Kangding-Yunnan land to the west, which was the main provenance area of the late Permian in western Guizhou. Transgressions came from the eastern and southern sides of the study area. The sedimentary facies units are distributed from northwest to southeast as continental facies−transitional facies−marine facies.[41,80,81] The various sedimentary facies gradually transition and are distributed in a pattern that is clearly controlled by the ancient topography of the western high and eastern low coal basins. The distribution of
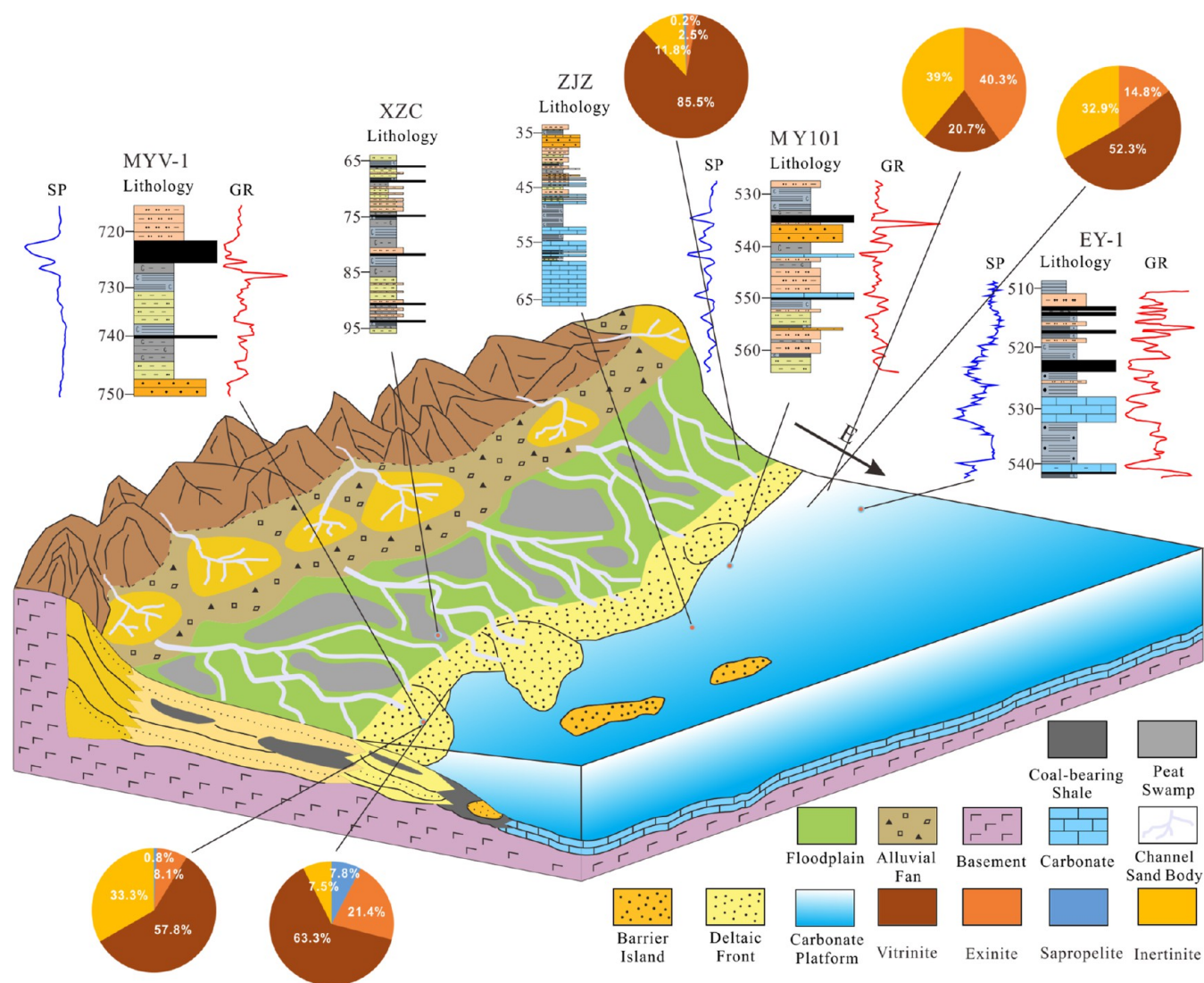
Figure 12. Sedimentary model map of the Longtan Formation in the study area, western Guizhou region.

continental sedimentary areas is located on the eastern edge of the ancient Kangdian-Yunnan land and contains mainly developing weathering residual plains, piedmont alluvial fans, river alluvial plains, and other facies types. The sedimentary system of marine−continental transitional areas includes the delta and tidal flat sedimentary systems, which are influenced by the sedimentary structures. Overall, the transitional area exhibits a north−south trending parallel distribution. The marine sedimentary area mainly consists of carbonate platforms and deepwater basins dominated by carbonates.[82]

The lower Permian shale in the western Guizhou area was deposited in a lagoon-tidal flat sedimentary environment under hypoxic conditions. The semirestricted, low hydrodynamic lagoon environment and gently sloping tidal flat environment provided an ideal environment for organic matter enrichment.[26] During this period, the study area was located in a low-latitude region, with a warm and humid climate that favored the growth of plants and microorganisms, which could provide a rich and diverse source of organic matter.[83,84] The organic macerals were mainly composed of exinite, relatively high contents of inertinite, and generally lower contents of vitrinite (Table 3), indicating a rich and diverse source of organic matter rather than a single source. During the upper Permian

period, river activity intensified, and the sedimentary environment changed to a delta, with a warm and humid paleoenvironment. The river mixed the terrigenous debris and terrestrial plant debris together and poured into the basin at a higher sedimentation rate. The delta plain (swamp) had a good environment for organic matter enrichment. The organic macerals were mainly composed of vitrinite, accounting for more than half of the total content, with lower contents of exinite and inertinite and a small amount of sapropelite (Table 3). This result indicates a single source and enrichment of organic matter, mainly from the terrigenous source area (Figure 12).

6. CONCLUSIONS

The total organic carbon content of the coal-bearing rock series of the Longtan Formation in western Guizhou was high, with an average TOC of 6.41% and a range of 1.44−14.79%. Most samples, approximately 78.6%, had TOC values exceeding 2%, indicating a potential for shale gas resources. The dominant organic matter was vitrinite, with type III kerogen. Clay minerals and brittle minerals constituted the mineral composition; kaolinite (average 11.13%) and illite−smectite mixed layers (average 26.69%) were the main constituents of

the clay minerals, and quartz (average 31.63%) and feldspar (average 12.88%) were the main constituents of the brittle minerals.

Eight typical lithofacies types were identified in the Longtan Formation in the western Guizhou study area; these included silty mudstone, muddy siltstone, carbonaceous mudstone, carbonaceous shale, bioclastic-bearing mudstone, bioclastic-bearing siltstone, fine sandstone, and coal seam. The first six were fine-grained sedimentary rocks.

Six typical lithofacies assemblages corresponding to different sedimentary environments were identified in the Longtan Formation in the western Guizhou region through observation of cores, thin section identification, and analysis of logging data. Lithofacies assemblage A consisted of muddy siltstone and silty mudstone; lithofacies assemblage B consisted of coal seam, carbonaceous mudstone, and carbonaceous shale; lithofacies assemblage C consisted of silty mudstone, carbonaceous mudstone, carbonaceous shale, and coal seam; lithofacies assemblage D consisted of fine sandstone, muddy siltstone, silty mudstone, carbonaceous mudstone, carbonaceous shale, and coal seam; lithofacies assemblage E consisted of fine sandstone, silty mudstone, muddy siltstone, carbonaceous mudstone, carbonaceous shale, and coal seam; and lithofacies assemblage F consisted of fine sandstone and coal seam.

The sedimentary environment of the Longtan Formation in the study area was found to be primarily a delta and tidal flat-lagoon sedimentary system dominated by marine−continental transitional facies environments.

AUTHOR INFORMATION

Corresponding Author

    Xuan Tang − *School of Energy Resources, China University of Geosciences, Beijing, Beijing 100083, China;* ⬤ orcid.org/0000-0002-6074-9633; Email: tangxuan@cugb.edu.cn

Authors

    Xiaoming Li − *School of Energy Resources, China University of Geosciences, Beijing, Beijing 100083, China;* ⬤ orcid.org/0009-0005-6336-3284

    Shaobin Guo − *School of Energy Resources, China University of Geosciences, Beijing, Beijing 100083, China*

    Jinchuan Zhang − *School of Energy Resources, China University of Geosciences, Beijing, Beijing 100083, China;* ⬤ orcid.org/0000-0002-2979-4866

    Ende Deng − *School of Energy Resources, China University of Geosciences, Beijing, Beijing 100083, China; Guizhou Energy Group Co., Ltd., Guiyang, Guizhou 550081, China*

    Chaoli Lan − *State Key Laboratory of Petroleum Resources and Prospecting and College of Petroleum Engineering, China University of Petroleum, Beijing 102249, China;* ⬤ orcid.org/0000-0002-1501-6983

Complete contact information is available at:
https://pubs.acs.org/10.1021/acsomega.3c03343

Notes

The authors declare no competing financial interest.

REFERENCES

(1) Dong, D.; Wang, Y.; Li, X.; Zou, C.; Guan, Q.; Zhang, C.; Huang, J.; Wang, S.; Wang, H.; Liu, H.; et al. Breakthrough and prospect of shale gas exploration and development in China. *Nat. Gas. Ind.* **2016**, *3*, 12−26. From Cnki

(2) Zou, C.; Dong, D.; Wang, Y.; Li, X.; Huang, J.; Wang, S.; Guan, Q.; Zhang, C.; Wang, H.; Liu, H.; et al. Shale gas in China: characteristics, challenges and prospects (II). *Petrol. Explor. Dev.* **2016**, *43*, 182−196. From Cnki

(3) Zou, C.; Zhao, Q.; Cong, L.; Wang, H.; Shi, Z.; Wu, J.; Pan, S. Development progress, potential and prospect of shale gas in China. *Nat. Gas. Ind.* **2021**, *41*, 1−14. From Cnki

(4) Wenzhi, Z.; Jia, A.; Wei, Y.; Wang, J.; Zhu, H. Progress in shale gas exploration in China and prospects for future development. *China Pet. Explor.* **2020**, *25*, 31−44. From Cnki

(5) Yue, P. S.; Shi, Q.; Yue, L.; Liang, Y. The latest progress of shale gas exploration and development in China. *Nat. Gas Explor. Dev.* **2017**, *40*, 38−44. From Cnki

(6) Ma, Y.; Cai, X.; Zhao, P. China's shale gas exploration and development: Understanding and practice. *Petrol. Explor. Dev.* **2018**, *45*, 589−603. From Cnki

(7) Zou, C.; Zhao, Q.; Dong, D.; Yang, Z.; Qiu, Z.; Liang, F.; Wang, N.; Huang, Y.; Duan, A.; Zhang, Q.; et al. Geological characteristics, main challenges and future prospect of shale gas. *Nat. Gas Geosci.* **2017**, *2*, 273−288. From Cnki

(8) Potter, C. J. Paleozoic shale gas resources in the Sichuan Basin, China. *AAPG Bull.* **2018**, *102*, 987−1009.

(9) Dong, D.; Shi, Z.; Guan, Q.; Jiang, S.; Zhang, M.; Zhang, C.; Wang, S.; Sun, S.; Yu, R.; Liu, D.; et al. Progress, challenges and prospects of shale gas exploration in the Wufeng−Longmaxi reservoirs in the Sichuan Basin. *Nat. Gas. Ind.* **2018**, *5*, 415−424. From Cnki

(10) Ma, X.; Guo, S. B.; Shi, D. S.; Zhou, Z.; Liu, G. H. Investigation of pore structure and fractal characteristics of marine-continental transitional shales from Longtan Formation using MICP, gas adsorption, and NMR (Guizhou, China). *Mar. Petrol. Geol.* **2019**, *107*, 555−571.

(11) Ma, X.; Guo, S. B. Comparative Study on Shale Characteristics of Different Sedimentary Microfacies of Late Permian Longtan Formation in Southwestern Guizhou, China. *Minerals* **2019**, *9*, 20.

(12) Deng, E.; Yan, Z.; Jiang, B.; Wang, R. Reservoir characteristics of marine-continental shale gas in Upper Permian Longtan Formation, western Guizhou province. *Pet. Geol. Exp.* **2020**, *42*, 467−476. From Cnki

(13) Deng, E.; Jiang, B.; Gao, W.; Fu, W. Study on pore structure and fractal characteristics of shale from coal measures of Longtan Formation in western Guizhou. *Coal Sci. Technol.* **2020**, *48*, 184−190.

(14) Huang, Y. Q.; Zhang, P.; Zhang, J. C.; Tang, X.; Liu, C. W.; Yang, J. W. Fractal Characteristics of Pores in the Longtan Shales of Guizhou, Southwest China. *Geofluids* **2020**, *2020*, 1−16.

(15) Wang, E.; Guo, T.; Liu, B.; Li, M.; Xiong, L.; Dong, X.; Zhang, N.; Wang, T. Lithofacies and pore features of marine-continental transitional shale and gas enrichment conditions of favorable lithofacies: A case study of Permian Longtan Formation in the Lintanchang area, southeast of Sichuan Basin, SW China. *Petrol. Explor. Dev.* **2022**, *49*, 1310−1322. From Cnki

(16) Zhai, G.; Wang, Y.; Liu, G.; Zhou, Z.; Zhang, C.; Liu, X. Enrichment and accumulation characteristics and prospect analysis of the Permian marine continental multiphase shale gas in China. *Sediment. Geol. Tethyan Geol.* **2020**, *40*, 102−117.

(17) Li, K.; Zhao, L.; Bai, L.; Deng, E. Study on shale gas accumulation conditions for Longtan formation of Upper Permia in western Guizhou. *Petrochem. Ind. Appl.* **2019**, *38*, 76−80. From Cnki

(18) Wang, P.; Liu, G.; Liu, Z.; Chen, X.; Li, P.; Cai, B. Shale gas enrichment conditions and controlling factors of Upper Permian Longtan Formation transitional shale in Southeast Sichuan to Northwest Guizhou. *Nat. Gas Geosci.* **2022**, *33*, 431−440. From Cnki

(19) Guo, S. B.; Wang, z.; Ma, X. Exploration prospect of shale gas with Permian transitional facies of some key areas in China. *Pet. Geol. Exp.* **2021**, *43*, 377−385. From Cnki

(20) Guo, S.; Fu, J.; Gao, D.; Li, H.; Huang, J. Research status and prospects for marine-continental shale gases in China. *Pet. Geol. Exp.* **2015**, *37*, 535−540. From Cnki

(21) Li, Q.; Xu, S. Research status and prospects of marine-continental transitional shale reservoirs. *Geol. Bull. China* **2022**, *41*, 1417−1429. From Cnki

(22) Jia, L.; Shu, J.; Jiang, Z.; Zhang, D.; Wang, B.; Du, T.; Zhu, W. Study on formation conditions and reservoir characteristics of marine-terrigenous facies coal measures shale gas in western Guizhou. *Coal Sci. Technol.* **2021**, *49*, 201−207.

(23) Cao, W.; He, J.; Yang, T.; Wang, J.; Shi, S.; Xing, H. Longtan Formation Sedimentary Environment and Its Control on Shale Development in Zhijin Area, Guizhou. *Coal Geology of China* **2021**, *33*, 25−31. From Cnki

(24) Luo, S.; Wang, L.; Shi, F.; Tang, X. Potentiality Exploration of the Longtan Formation Coal Shale Gas in Southwestern Guizhou Province. *Sci. Technol. Eng.* **2017**, *17*, 162−168. From Cnki

(25) Wang, H.; Shao, L.; Hao, L.; Zhang, P.; Glasspool, I. J.; Wheeley, J. R.; Wignall, P. B.; Yi, T.; Zhang, M.; Hilton, J. Sedimentology and sequence stratigraphy of the Lopingian (Late Permian) coal measures in southwestern China. *Int. J. Coal Geol.* **2011**, *85*, 168−183.

(26) Liu, S. X.; Wu, C. F.; Li, T.; Wang, H. C. Multiple geochemical proxies controlling the organic matter accumulation of the marine-continental transitional shale: A case study of the Upper Permian Longtan Formation, western Guizhou, China. *J. Nat. Gas Sci. Eng.* **2018**, *56*, 152−165.

(27) Zhang, Q.; Grohmann, S.; Xu, X. C.; Littke, R. Depositional environment and thermal maturity of the coal-bearing Longtan Shale in southwest Guizhou, China: Implications for shale gas resource potential. *Int. J. Coal Geol.* **2020**, *231*, 103607.

(28) Sun, C.; Xu, H.; Tang, D.; Xin, F.; Ren, P.; Cao, L. Sequence-depositional characteristics and coal accumulation patterns of Longtan coal strata in northwestern Guizhou. *Sci. Technol. Eng.* **2018**, *18*, 46−55. From Cnki

(29) Luo, W.; Hou, M. C.; Liu, X. C.; Huang, S. G.; Chao, H.; Zhang, R.; Deng, X. Geological and geochemical characteristics of marine-continental transitional shale from the Upper Permian Longtan formation, Northwestern. Guizhou, China. *Mar. Petrol. Geol.* **2018**, *89*, 58−67.

(30) He, Q.; Dong, T.; He, S.; Zhai, G. Y.; Guo, X. W.; Hou, Y. G.; Yang, R.; Han, Y. J. Sedimentological and geochemical characterization of the Upper Permian transitional facies of the Longtan Formation, northern Guizhou Province, southwest China: Insights into paleo-environmental conditions and organic matter accumulation mechanisms. *Mar. Petrol. Geol.* **2020**, *118*, 104446.

(31) He, Y.; Tang, X.; Shan, Y.; Liu, G.; Xie, H.; Ma, Z. Lithofacies division and comparison and characteristics of Longtan Formation shale in typical areas of Sichuan Basin and its surrounding. *Nat. Gas Geosci.* **2021**, *32*, 174−190. From Cnki

(32) Xiao, W.; Zhang, B.; Yao, Y.; Wang, Y.; Yang, H.; Yang, K. Lithofacies and sedimentary environment of shale of Permian Longtan Formation in eastern Sichuan Basin. *Lithol. Reservoirs* **2022**, *34*, 152.

(33) Wang, G. P.; Jin, Z. J.; Hu, Z. Q.; Liu, G. X.; Zhu, T.; Du, W.; Wang, H. L.; Wu, J. Sedimentary Evolution Characteristics of Fine-Grained Lithofacies under the High-Resolution Isochronous Shelf System: Insights from the Wufeng-Longmaxi Shales in the Sichuan Basin. *Lithosphere* **2021**, *2021*, 6628867.

(34) Zhao, J.; Jin, Z.; Jin, Z.; Wen, X.; Geng, Y.; Yan, C.; Nie, H. Lithofacies types and sedimentary environment of shale in Wufeng-Longmaxi Formation, Sichuan Basin. *Acta Pet. Sin.* **2016**, *37*, 572−586. From Cnki

(35) Yu-Man, W.; Wang, S.; Dong, D.; Li, X.; Huang, J.; Zhang, C.; Guan, Q. Lithofacies characterization of Longmaxi Formation of the lower Silurian. southern Sichuan. *Earth Sci. Front.* **2016**, *23*, 119−133.

(36) Ozkan, A.; Cumella, S. P.; Milliken, K. L.; Laubach, S. E. Prediction of lithofacies and reservoir quality using well logs, Late Cretaceous Williams Fork Formation, Mamm Creek field, Piceance Basin, Colorado. *AAPG Bull.* **2011**, *95*, 1699−1723.

(37) Loucks, R. G.; Ruppel, S. C. Mississippian Barnett Shale: Lithofacies and depositional setting of a deep-water shale-gas succession in the Fort Worth Basin, Texas. *AAPG Bull.* **2007**, *91*, 579−601.

(38) Hickey, J. J.; Henk, B. Lithofacies summary of the Mississippian Barnett Shale, Mitchell 2 T.P. Sims well, Wise County, Texas. *AAPG Bull.* **2007**, *91*, 437−443.

(39) Deng, E.; Zhang, Q.; Jin, Z.; Zhu, R.; Yan, Z.; Jiang, B.; Littke, R. Non-overmature equivalents confirmed a high initial hydrocarbon generation potential of the Permian Longtan Shale in southern China. *Int. J. Coal Geol.* **2022**, *259*, 104043.

(40) Province, G. S. A. o. G. *The Regional Geology of China*; Geological Publishing House: Guizhou Province, 2017.

(41) Dou, X. Z.; Jiang, B.; Qin, Y.; Wang, W.; Chen, W. Structure Evolution in West of Guizhou Area and Control to Seam in Late Permian. *Coal Sci. Technol.* **2012**, *40*, 109−114.

(42) Li, A.; Ding, W. L.; Jiu, K.; Wang, Z.; Wang, R. Y.; He, J. H. Investigation of the pore structures and fractal characteristics of marine shale reservoirs using NMR experiments and image analyses: A case study of the Lower Cambrian Niutitang Formation in northern Guizhou Province, South China. *Mar. Petrol. Geol.* **2018**, *89*, 530−540.

(43) Dou, X.; Jiang, B.; Qin, Y.; Qu, Z.; Li, M. Tectonic Control of Coalbed Methane Reservoirs in Panxian, Western Guizhou. *Geol. J. China Univ.* **2012**, *18*, 447−452.

(44) Ma, X.; Guo, S. Study on pore evolution and diagenesis division of a Permian Longtan transitional shale in Southwest Guizhou, China. *Energy Sci. Eng.* **2021**, *9*, 58−79.

(45) Dou, X. Tectonic Evolution and Its Control on Coalbed Methane Reservoiring in Western Guizhou. Doctor of Engineering, China University of Mining & Technology, Beijing, Beijing, 2012.

(46) Yue, G.; Zhang, S.; Yang, W. Structural Deformation Patterns and Tectonic Stress Field in West-Central Guizhou. *Chin. J. Geol.* **1994**, *29*, 10−18. From Cnki

(47) Ma, X. Fine characterization of shale reservoir of Longtan Formation in western Guizhou. Doctor of Engineering, China University of Geosciences Beijing, Beijing, 2021.

(48) Wang, H. Sedimentological characteristics and palaeoenvironmental bearings of the Late Permian coals in eastern Yunnan and western Guizhou of southwestern China. Doctor of Engineering, China University of Mining & Technology, Beijing, Beijing, 2011.

(49) Yue, H.; Chang, H.; Fan, Y.; Chen, F.; Chen, P. Construction and prospect of China's shale gas technical standard system. *Nat. Gas. Ind.* **2020**, *7*, 664−670.

(50) Zhou, Y.; Rui, X.; Bao, F.; Yu, L.; Zhang, Q.; Xi, B. Thermal Maturity and Pore Characteristics of Jurassic Continental Shale in Sichuan Basin. *J. Xi'an Shiyou Univ. (Natural Science Edition)*, **2023**, *38* (3), 27−37, 80.

(51) Peng, J.; Yu, L. D.; Xu, T. Y.; Wang, Y. B.; Han, H. D. Analysis of Sedimentary Environment Conditions for Lacustrine Fine-Grained Sedimentary Rocks and Its Control of Lithofacies Development: A Case Study of the Lower Submember of Member 3 of Shahejie Formation in FY-1 Well, Dongying Sag, Bohai Bay Basin, China. *Geofluids* **2021**, *2021*, 1−16.

(52) Wang, G.; Jin, Z.; Zhang, Q.; Zhu, R.; Tang, X.; Liu, K.; Dong, L. Effects of clay minerals and organic matter on pore evolution of the early mature lacustrine shale in the Ordos Basin, China. *J. Asian Earth Sci.* **2023**, *246*, 105516.

(53) Li, S.; Zhu, R.; Cui, J.; Luo, Z.; Jiao, H.; Liu, H. Sedimentary Characteristics of Fine - grained Sedimentary Rock and Paleo - environment of Chang 7 Member in the Ordos Basin: A case study from Well Yaoye 1 in Tongchuan. *Acta Sedimentol. Sin.* **2019**, *38*, 1−13.

(54) Liu, Y. Y.; Wilcox, J. Molecular simulation of CO2 adsorption in micro- and mesoporous carbons with surface heterogeneity. *Int. J. Coal Geol.* **2012**, *104*, 83−95.

(55) Karayigit, A. I.; Mastalerz, M.; Oskay, R. G.; Buzkan, I. Bituminous coal seams from underground mines in the Zonguldak Basin (NW Turkey): Insights from mineralogy, coal petrography, Rock-Eval pyrolysis, and meso-and microporosity. *Int. J. Coal Geol.* **2018**, *199*, 91−112.

(56) Mastalerz, M.; He, L. L.; Melnichenko, Y. B.; Rupp, J. A. Porosity of Coal and Shale: Insights from Gas Adsorption and SANS/USANS Techniques. *Energy Fuel.* **2012**, *26*, 5109−5120.

(57) Weniger, P.; Kalkreuth, W.; Busch, A.; Krooss, B. M. High-pressure methane and carbon dioxide sorption on coal and shale samples from the Parana Basin, Brazil. *Int. J. Coal Geol.* **2010**, *84*, 190−205.

(58) Shaobin, G.; Wang, Y. Shale gas accumulation conditions and exploration potential of Carboniferous Benxi Formation in Ordos Basin. *Acta Pet. Sin.* **2013**, *34*, 445−452. From Cnki

(59) Xue, C. Q.; Wu, J. G.; Qiu, L. W.; Zhong, J. H.; Zhang, S. R.; Zhang, B.; Wu, X.; Hao, B. Lithofacies classification and its controls on the pore structure distribution in Permian transitional shale in the northeastern Ordos Basin, China. *J. Petrol. Sci. Eng.* **2020**, *195*, 107657.

(60) Wang, F. T.; Guo, S.; Mao, W.; Peng, Y. Evolution of clay mineral and the division of diagenesis stages in mud shale based on thermal simulation. *Sci. Technol. Eng.* **2018**, *18*, 174−179. From Cnki

(61) Yang, C.; Zhang, J. C.; Tang, X.; Ding, J. H.; Zhao, Q. R.; Dang, W.; Chen, H. Y.; Su, Y.; Li, B. W.; Lu, D. F. Comparative study on micro-pore structure of marine, terrestrial, and transitional shales in key areas, China. *Int. J. Coal Geol.* **2017**, *171*, 76−92.

(62) Liu, H.; Zhang, S.; Wang, X.; Zhang, P.; Li, J.; Wang, Y.; Wei, X.; Yin, Y.; Zhu, D. Types and Characteristics of Shale Lithofacies Combinations in Continental Faulted Basins: A Case Study from Upper Sub-Member of Es4 in Dongying Sag, Jiyang Depression. *Earth Sci. J. China Univ. Geosci.* **2023**, *48* (1), 30−48.

(63) Feng, Z. Some new thoughts on definitions of terms of sedimentary facies: based on Miall's paper (1985). *J. Palaeogeogr.* **2022**, *11*, 1−7 From Cnki.

(64) Feng, Z. Z. A review on the definitions of terms of sedimentary facies. *J. Palaeogeogr.* **2019**, *8*, 32. From Cnki

(65) Wang, G.; Jin, Z.; Liu, G.; Wang, R.; Zhao, G.; Tang, X.; Liu, K.; Zhang, Q. Pore system of the multiple lithofacies reservoirs in unconventional lacustrine shale oil formation. *Int. J. Coal Geol.* **2023**, *273*, 104270.

(66) Peng, S. Z.; Liu, D.; Zhang, L.; Qiu, Z.; Wang, Y.; Feng, C.; Sun, M. Shale Lithofacies and Sedimentary Facies of the Permian Shanxi Formation, Daning-Jixian Area, Eastern Margin of Ordos Basin. *Acta Sedimentol. Sin.* **2022**, *40*, 47−59.

(67) Vandenbroucke, M.; Largeau, C. Kerogen origin, evolution and structure. *Org. Geochem.* **2007**, *38*, 719−833.

(68) Rimmer, S. M.; Davis, A. The influence of depositional environments on coal petrographic composition of the Lower Kittaning seam, western Pennsylvania. *Org. Geochem.* **1988**, *12*, 375−387.

(69) Miceli Romero, A.; Philp, R. P. Organic geochemistry of the Woodford Shale, southeastern Oklahoma: How variable can shales be? *AAPG Bull.* **2012**, *96*, 493−517.

(70) Crosdale, P. J. Coal maceral ratios as indicators of environment of deposition: do they work for ombrogenous mires? An example from the Miocene of New Zealand. *Org. Geochem.* **1993**, *20*, 797−809.

(71) Chen, Z. *Petroleum and Natural Gas Geology*; Geological Publishing House, 2005.

(72) Xi, Z. D.; Tang, S. H.; Wang, J.; Yi, J. J.; Guo, Y. Y.; Wang, K. F. Pore Structure and Fractal Characteristics of Niutitang Shale from China. *Minerals* **2018**, *8*, 163.

(73) Wang, G.; Zhang, Q.; Zhu, R.; Tang, X.; Liu, K.; Jin, Z. Geological controls on the pore system of lacustrine unconventional shale reservoirs: The Triassic Chang 7 member in the Ordos Basin, China. *Geoenergy Sci. Eng.* **2023**, *221*, 111139.

(74) Changpeng, Y. F.; Ning, Z.; Hu, C.; Wang, B.; Peng, K.; Liu, H. Characterization of microscopic pore structures in shale reservoirs. *Acta Pet. Sin.* **2013**, *34*, 301−311. From Cnki

(75) Bustin, R.; Bustin, A.; Ross, D.; Chalmers, G.; Cui, X. Shale gas opportunities and challenges. *Search Discov. Artic.* **2009**, *40382*, 20−23.

(76) Tian, C.; Le, C.; Zhang, R.; Zhang, P.; Xu, J. Study of Lithofacies Associations and Sedimentary Environments of Lower-Middle Triassic Carbonate Rocks in Shimen Region, Hunan, China. *Earth Sci.* **1997**, *03*, 78−82. From Cnki

(77) Gao, C. Sedimentary Characteristics and Depositional Model of Fluvial Fan with Far Provenances- A Case Study of Modern Baiyanghe Alluvial Fan in Northern Margin of Heshituoluogai Basin. Doctor of Engineering, China University of Petroleum, Beijing, Beijing, 2018.

(78) Jiao, Y. Sedimentary Characteristics and the Formation Conditions of Fine-grained Mixed Sedimentary Rocks in the Second Member of Kongdian Formation in Cangdong Sag. M.Sc. Thesis, China University of Petroleum (East China), Qingdao, Shandong Province, 2017.

(79) Zhao, Z. Coupling Relationship of Structure-Sedimentation-Diagenesis and Its Effect on Reservoir Quality Controlling in the Huagang Formation of "X" Gas Field in the Xihu Sag. Doctor of Engineering, China University of Petroleum (East China), Qingdao, Shandong Province, 2019.

(80) Shao, L. Y.; Gao, C.; Zhang, C.; Wang, H.; Guo, L.; Gao, C. Sequence-Palaeogeography and Coal Aaccumulation of Late Permian in Southwestern China. *Acta Sedimentol. Sin.* **2013**, *31*, 856−866.

(81) Shao, L.; Liu, H.; Tian, B.; Zhang, P. Sedimentary Evolution and its Controls on Coal Accumulation for the Late Permian in the Upper Yangtze Area. *Acta Sedimentol. Sin.* **1998**, *16*, 55−60. From Cnki

(82) Gao, C. Sequence-palaeogeography and Coal-accumulation of Late Permian in Chuan-Yu-Dian-Qian, China. Doctor of Engineering, China University of Mining & Technology, Beijing, 2015.

(83) Junda, W.; Huamei, L. Paleo-latitude variation of Guizhou terrain from Devonian to Cretaceous. *Chin. J. Geochem.* **1998**, *17*, 356−361. From Cnki

(84) Rees, P. M.; Ziegler, A. M.; Gibbs, M. T.; Kutzbach, J. E.; Behling, P. J.; Rowley, D. B. Permian phytogeographic patterns and climate data/model comparisons. *J. Geol.* **2002**, *110*, 1−31.